Studies on cell tropism of hemorrhagic fever viruses and mechanisms of entry into cells
(出血熱ウイルスの細胞指向性と細胞侵入メカニズムに関する研究)

Takeshi SAITO

Contents

Abbreviations

α-DG	α-dystroglycan
ALP	alkaline phosphatase
ALT	alanine aminotransferase
ANOVA	one-way repeated-measures analysis
AST	aspartate aminotransferase
BHK	baby hamster kidney
BSL	biosafety level
DC/L-SIGN	dendritic cell- and liver/lymph node-specific ICAM-3-grabbing non-integrin
DMEM	Dulbecco's modified Eagle's medium
DNP	2,4-dinitrophenol
dpi	days post-infection
EBOV	Ebola virus
EDTA	ethylenediaminetetraacetic acid
ELISA	enzyme-linked immunosorbent assay
EVD	Ebola virus disease
FCS	fetal calf serum
G	glycoprotein
GFP	green fluorescent protein
GP	glycoprotein
GRA	granulocyte
HA	hemagglutinin
HCV	hepatitis C virus
HE	hematoxylin and eosin
HEK	human embryonic kidney
hMGL	human macrophage galactose-type C-type lectin
HRP	horseradish peroxidase
i.p.	intraperitoneally
IFN	interferon
IFNAR	interferon-α/β receptor

IHC	immunohistochemistry
IRES	internal ribosome entry site
IU	infectious unit
L	RNA-dependent RNA polymerase
LAMP1	lysosomal-associated membrane protein 1
LASV	Lassa virus
LD_{50}	50% lethal dose
LDL	low-density lipoprotein
LEL	large extracellular loop
LSECtin	liver and lymph node sinusoidal endothelial cell C-type lectin
LUJV	Lujo virus
LYM	lymphocyte
MAb	monoclonal antibody
MA-EBOV	mouse-adapted EBOV
MARV	Marburg virus
MON	monocyte
MVD	Marburg virus disease
NHP	nonhuman primate
NPC1	Niemann-Pick C1
NRP2	neuropilin-2
NW	New World
OW	Old World
PBS	phosphate-buffered saline
PBST	PBS containing 0.05% Tween 20
PCR	polymerase chain reaction
PFU	plaque-forming unit
PLT	platelet
PVDF	polyvinylidene fluoride
RBC	red blood cell
rVSV	replication-competent recombinant VSV
SDS-PAGE	Sodium dodecyl sulfate-polyacrylamide gel electrophoresis

SEL	small extracellular loop
STAT	signal transducer and activator of transcription
TfR1	transferrin receptor-1
TM	transmembrane domain
VP	viral protein
VSV	vesicular stomatitis viruses
WBC	white blood cell
WT	wild-type
Z	matrix protein

Notes

The contents of Chapter I have been published in *Viruses*.

Saito T, Maruyama J, Nagata N, Isono M, Okuya K, Takadate Y, Kida Y, Miyamoto H, Mori-Kajihara A, Hattori T, Furuyama W, Ogawa S, Iida S, Takada A. A Surrogate Animal Model for Screening of Ebola and Marburg Glycoprotein-Targeting Drugs Using Pseudotyped Vesicular Stomatitis Viruses. *Viruses* 12(9), 923, 2020.

Preface

Most of the viruses that cause viral hemorrhagic fevers in humans are taxonomically divided into several families; *Filoviridae*, *Arenaviridae*, *Flaviviridae*, *Nairoviridae*, *Hantaviridae*, *Phenuiviridae*, and *Paramyxoviridae*, all of which include enveloped RNA viruses [1,2]. Clinically approved vaccines or antiviral drugs against viral hemorrhagic fevers are only limitedly available [3–6] and some of these viruses are classified as biosafety level (BSL)-4 pathogens. Filoviruses, represented by Ebola virus (EBOV) and Marburg virus (MARV), are known to cause severe hemorrhagic fever in humans and nonhuman primates (NHPs) [6–8]. Arenaviruses such as Lassa virus (LASV) and Lujo virus (LUJV) are distributed in African continent and also known cause fatal hemorrhagic fevers in humans [9–11]. In order to take counter measures against these hemorrhagic fever viruses, it is important to understand the mechanisms underlying their pathogenicity and etiology.

On the surface of filovirus and arenavirus particles, there are envelope glycoproteins (GPs) which are responsible for viral entry into cells [6,8,9,12,13]. In the initial step of the entry, GPs bind to their attachment receptors on host cell surfaces. T-cell immunoglobulin and mucin domain 1 and C-type lectins such as dendritic cell- and liver/lymph node-specific ICAM-3-grabbing non-integrin (DC/L-SIGN), human macrophage galactose-type C-type lectin (hMGL), and liver and lymph node sinusoidal endothelial cell C-type lectin (LSECtin) are known to be attachment receptors of filoviruses [14,15]. On the other hand, alpha-dystroglycan (α-DG) and neuropilin-2 (NRP2) are reported as attachment receptors of LASV and LUJV, respectively [9,16–19]. After incorporation of viral particles into cellular endosomes, EBOV, MARV, LASV, and LUJV need to interact with their intracellular receptors for membrane fusion between viral envelope and cell membrane. Niemann-Pick C1 (NPC1) is the intracellular receptor of filoviruses [20,21]. LASV and LUJV utilize lysosomal-associated membrane protein 1 (LAMP1) and CD63 as intracellular receptors, respectively [16,22,23].

Since GPs are essential for virus entry into cells, they are important targets of neutralizing antibodies and antiviral candidate compounds that block the interaction of GPs to the respective receptors [24–26]. It is also worthy to note that the interaction between GPs and their receptors is generally a primary determinant for viral tissue tropism. Interestingly, the intracellular receptors are also thought to be involved in host range restriction of filoviruses and arenaviruses [19,27–33]. For example, variation of NPC1 among cell lines derived from different animal species have been shown to affect susceptibilities to filoviruses [27,28,30]. To understand the pathogenicity and etiology of these viruses, it is important to analyze the function and property of GPs.

The development of anti-EBOV or -MARV drugs has been hampered by the restriction requiring BSL-4 facility for handling infectious filoviruses. In chapter I, a surrogate animal model that can be conducted under BSL-2 or -3 conditions was established. I used Syrian hamsters infected with a replication competent vesicular stomatitis virus (rVSV) bearing EBOV or MARV GP (rVSV/EBOV or rVSV/MARV, respectively) and investigated GP-dependent tropisms and pathogenesis. I further confirmed the usefulness of this model for screening of anti-EBOV drugs targeting GPs.

In chapter II, I focused on the role of GP in the host range restriction of LUJV using replication-incompetent VSV pseudotyped wtih LUJV GP (VSVΔG-LUJV/GP). Differential susceptibilities to LUJV infection among animal species or cell lines were reported [34–36]; however the molecular mechanisms of the tissue tropism and host range of LUJV is still unknown. In the present study, susceptibility to VSVΔG-LUJV/GP was compared among human- and rodent-derived cell lines and the molecular determinant for the differential susceptibilities of the cell lines were analyzed.

Chapter I:

A Surrogate Animal Model for Screening of Ebola and Marburg Glycoprotein-Targeting Drugs Using Pseudotyped Vesicular Stomatitis Viruses

Introduction

The family *Filoviridae* includes five genera: *Ebolavirus*, *Marburgvirus*, *Cuevavirus*, *Striavirus*, and *Thamnovirus*. The *Ebolavirus* genus contains five species—*Zaire ebolavirus* represented by Ebola virus (EBOV), *Sudan ebolavirus*, *Taï Forest ebolavirus*, *Bundibugyo ebolavirus*, and *Reston ebolavirus*. The *Marburgvirus* genus consists of only one species, *Marburg marburgvirus* including the prototype filovirus, Marburg virus (MARV) [7]. The filovirus genome encodes seven structural proteins, an envelope glycoprotein (GP), a nucleoprotein, viral proteins (VP24, VP30, VP35, and VP40), and L protein. GP is the only viral surface protein of filoviruses and mediates attachment of virus particles to host cells and fusion of the viral envelope with the host cell membrane, which is the initial step of virus infection [6,8,12].

Except for Reston virus, members of genera *Ebolavirus* and *Marburgvirus* are known to cause severe hemorrhagic fever in humans and NHPs with high mortality rates. The diseases caused by EBOV and MARV are known as Ebola virus disease (EVD) and Marburg virus disease (MVD), respectively [6,37,38]. Animal models of EVD and MVD have been developed in mice, rats, guinea pigs, hamsters, ferrets, and NHPs [39–43]. Of these, EBOV and MARV infections of NHPs are the gold-standard models because they best represent similar pathogenesis of EVD or MVD in humans [8,43]. Thus, the NHP model has been used for experimental studies of EBOV and MARV pathogenicity and for the development of vaccines and antiviral drugs [44–48]. However, the use of NHPs in a high-biocontainment laboratory is associated with high cost and technical difficulties; hence, some rodent models have been developed to deal with these problems [41,49–52].

Since wild-type EBOV (WT-EBOV) and MARV do not cause fatal disease in immunocompetent mice and guinea pigs, mouse-adapted EBOV (MA-EBOV) and MARV, and guinea-pig adapted EBOV and MARV, all of which cause lethal infection uniformly in these animals, have been generated by serial passage of the viruses [51,53–56]. Immunocompromised mice [interferon (IFN)-α/β receptor-knockout (*IFNAR*$^{-/-}$) and transcription factor signal transducer and activator of transcription (STAT1)-knockout (*STAT1*$^{-/-}$) mice] are also used as alternative models since they are highly susceptible to WT-EBOV [57]. It has also been shown that infection of Syrian hamsters with MA-EBOV is a good model that gives increased coagulopathy, which is not generally

observed in the other rodent models [58]. However, due to the requirement of BSL-4 facilities for handling infectious EBOV and MARV, the currently available animal models have limitations of their use for early-stage screening of anti-EBOV and MARV drugs.

In this study, I evaluated replication-competent recombinant vesicular stomatitis viruses pseudotyped with EBOV and MARV GPs (rVSV/EBOV and rVSV/MARV, respectively) to determine their utility as surrogate viruses for *in vivo* drug screening under BSL-2 conditions [59–61]. These viruses were shown to be highly potent live attenuated vaccine candidates against EVD and MVD in rodent and NHP models [62,63] and the rVSV/EBOV-based vaccine has been clinically approved in the EU and USA [4,5]. On the other hand, rVSV/EBOV was reported to cause lethal infection in *IFNAR*$^{-/-}$ or *STAT1*$^{-/-}$ mice and neonatal mice [64], suggesting its potential to cause disease in some animals. This chapter demonstrates that intraperitoneal inoculation of Syrian hamsters with rVSV/EBOV and rVSV/MARV induces acute and fatal infection and that rVSV/EBOV-infected animals can be completely protected by passive immunization with a neutralizing antibody specific to EBOV GP. These rVSV/EBOV- and rVSV/MARV-infected Syrian hamster models may be useful for *in vivo* screening of anti-filovirus drugs that target the GP functions.

Materials and Methods

Cells and Viruses

Vero E6 cells were grown in Dulbecco's modified Eagle's medium (DMEM) (Sigma) supplemented with 10% fetal calf serum (FCS) (Sigma), 100 U/mL penicillin, and 0.1 mg/mL streptomycin (Gibco). Replication-competent recombinant VSVs (rVSV/VSV) (strain Indiana) and rVSV pseudotyped with EBOV (strain Mayinga) and MARV (strain Angola) GPs (rVSV/EBOV and rVSV/MARV, respectively) were generated as described previously [59,60]. Briefly, BHK-T7-Ito cells were cotransfected with a plasmid containing the recombinant VSV genome and plasmids expressing the VSV nucleoprotein (pCAGGS-VSV N), phosphoprotein (pCAGGS-VSV P), or polymerase (pCAGGS-VSV L) for the viral ribonucleoprotein constituents. After 48 hours at 37°C, supernatants were blind passage onto Vero E6 cells. Recovery of infectious virus was confirmed by observation for cytopathic effect. Rescued rVSV/VSV, rVSV/EBOV, and rVSV/MARV were propagated in Vero E6 cells and stored at –80 °C until use. Virus titers were determined by a plaque assay and represented as plaque-forming units (PFU). The use of VSVs was approved by the Committee for Safety Management of Pathogens, Research Center for Zoonosis Control, Hokkaido University (10[06]). The generation of recombinant VSVs and plasmids was approved by the Ministry of Education, Culture, Sports, Science, and Technology, Japan.

Monoclonal Antibodies

Based on the nucleotide sequence encoding the anti-EBOV GP neutralizing monoclonal antibody (MAb) 6D6 [65], a human–mouse chimeric MAb (ch6D6) was generated. Briefly, the VH and VL coding regions of 6D6 were separately cloned into in-house-developed expression vectors for human IgG1 heavy chain and human kappa light chain, respectively (vector information is strictly restricted under a licensing agreement). The obtained constructs were transfected into Expi293F™ cells (Invitrogen), and antibodies were purified from the supernatants using Protein A-conjugated Sepharose columns (GE Healthcare). An anti-2,4-dinitrophenol (DNP) chimeric antibody was prepared similarly as a negative control, using a mouse anti-DNP antibody [66].

Experimental Infection of Rats, Mice, and Hamsters

All animal studies were carried out in strict accordance with the Guidelines for Proper Conduct of Animal Experiments of the Science Council of Japan. The protocol was approved (18-0026) by the Hokkaido University Animal Care and Use Committee. Six-week-old male F344/N rats, 6-week-old male BALB/c mice, and 6- or 3-week-old

male Syrian hamsters were purchased from Sankyo Lab Service. All animals were housed in animal BSL-2 or BSL-3 facilities in the Research Center for Zoonosis Control, Hokkaido University.

For the initial experiment, 6 rats, 6 mice, and 6 hamsters were inoculated intraperitoneally (i.p.) with rVSV/EBOV (10^7, $10^{6.5}$, and $10^{7.2}$ PFU, respectively) in a total volume of 300, 100, and 500 μL, respectively, and 3 animals from each group were euthanized on 2 days post-infection (dpi) for tissue sampling, and the remaining 3 animals were weighed daily for 8 dpi. Surviving animals were euthanized at 8 dpi. and serum samples were collected for antibody detection. To determine the 50% lethal dose (LD_{50}), four groups of 6-week-old male Syrian hamsters were infected i.p. with rVSV/EBOV (10^3–10^6 PFU) or rVSV/VSV (10^3–10^6 PFU) in a total volume of 200 μL and monitored for 7 dpi. Three groups of three 6-week-old Syrian hamsters were also infected i.p. with rVSV/MARV ($10^{5.5}$–$10^{7.5}$ PFU) in a total volume of 500 μL and monitored for 7 dpi. To investigate virus replication in hamsters, each group (of four 3-week-old hamsters) was infected i.p. with 10^7 PFU of rVSV/EBOV, rVSV/MARV, or rVSV/VSV in a total volume of 1,000 μL. All surviving animals were euthanized 36 hours after infection and tissue samples were collected from euthanized and deceased animals for virus titration and histopathological analysis. To analyze the changes in blood cell counts and blood chemistry, each group (of four 3-week-old hamsters) was infected i.p. with 10^7 PFU of rVSV/EBOV, rVSV/MARV, or rVSV/VSV in a total volume of 1,000 μL. All animals were euthanized 12 hours after infection and blood samples were collected.

Virus Titration

Virus titers were determined by plaque assays. Briefly, confluent Vero E6 cells in 12-well plates were inoculated with 10-fold serial dilutions of 10% tissue homogenates and incubated for 1 hour at 37 °C with 5% CO_2. After the inoculum was removed, the cells were washed with DMEM and overlaid with Eagle's minimum essential medium containing 0.8% Bacto Agar (Becton Dickinson). After 48 hours of incubation, cells were fixed with 10% formalin and stained with crystal violet. Virus titers were determined as PFU.

Histology and Immunohistochemistry

Liver, spleen, kidney, heart, lung, brain, salivary gland, testis, and colon samples were fixed in 10% neutral buffered formalin. The samples were trimmed, embedded in paraffin, sectioned at 5 μm with a microtome, placed on glass slides, and stained with hematoxylin and eosin (HE). The presence of viral antigens in tissues was also

investigated by a conventional immunohistochemistry (IHC) technique using HE-unstained sections. Slides were deparaffined in xylene and rehydrated through a series of graded ethanol. Endogenous peroxidase activity was blocked by incubation in 3% hydrogen peroxide in methanol for 10 min. The sections were washed twice in phosphate-buffered saline (PBS) and incubated with 10% normal goat serum [Histofine SAB-PO (R) kit, Nichirei Corporation] for 30 min. Then, they were exposed overnight to a rabbit anti-VSV N polyclonal antibody (in house) at a dilution of 1:1,000 at 4 ℃. After washing with PBS, a biotinylated goat antibody to rabbit immunoglobulin [Histofine SAB-PO (R) kit] was applied, followed by incubation at room temperature for 60 min. The immunohistochemical reactions were developed in freshly prepared 3,3'-diamino-benzidine tetrahydrochloride [Histofine SAB-PO (R) kit]. Slides were counterstained with hematoxylin and coverslipped in a mounting medium.

Hematology and Blood Biochemistry

Whole blood samples collected in EDTA (ethylenediaminetetraacetic acid) tubes were used for standard hematologic analysis using VETSCAN HM2 (ABAXIS) according to the manufacturer's instructions. The numbers of the following cell types were counted: white blood cells (WBC), red blood cells (RBC), platelets (PLT), monocytes (MON), lymphocytes (LYM), and granulocytes (GRA). Blood biochemistry analysis was performed with VETSCAN VS2 (ABAXIS). The following parameters were measured: alanine aminotransferase (ALT), aspartate aminotransferase (AST), and alkaline phosphatase (ALP).

Passive Immunization of Hamsters with Neutralizing Antibody ch6D6

Three-week-old Syrian hamsters (Sankyo Lab Service) were treated i.p. with 100 μg of MAb ch6D6 one day before or one hour after virus challenge with rVSV/EBOV (10^7 PFU), rVSV/MARV (10^7 PFU), or rVSV/VSV (10^7 PFU). An irrelevant Mab, chDNP, was used as a negative control antibody. The hamsters were monitored for signs of illness and their body weights were measured daily for 8 days. The animals were euthanized once they showed neurological signs such as paralysis and/or more than 20% body weight loss based on their baseline measurement at the time of virus inoculation.

Statistical Analysis

All data were analyzed using GraphPad Prism v6.0 software. To assess the whole blood counts and liver parameter changes, I performed a one-way repeated-measures analysis of variance (ANOVA), followed by multiple *t*-tests comparing the average

numbers of blood counts and liver parameters using the Tukey method. P values less than 0.05 were considered to be statistically significant.

Results

Different Susceptibility to rVSV/EBOV among Rodents

First, the susceptibilities of F344/N rats, BALB/c mice, and Syrian hamsters to rVSV/EBOV were compared. Groups of three rats, mice, and hamsters were inoculated with high doses of rVSV/EBOV (10^7, $10^{6.5}$, and $10^{7.2}$ PFU, respectively) *via* i.p. injection and monitored for signs of illness and body weight changes after infection. All of the rats and mice survived up to the end of the experiment and none of them showed body weight loss (Figure 1A, B). Using an enzyme-linked immunosorbent assay (ELISA), I detected high titers (> 10,000) of EBOV GP-specific IgG antibodies in serum samples collected from the surviving animals (data not shown), indicating that these animals were asymptomatically infected with the virus. In contrast, rVSV/EBOV-infected hamsters showed significant body weight loss and succumbed at 2 or 3 dpi (Figure 1C). These data indicated that rats, mice, and hamsters were susceptible to rVSV/EBOV, and that the virus caused lethal disease only in hamsters.

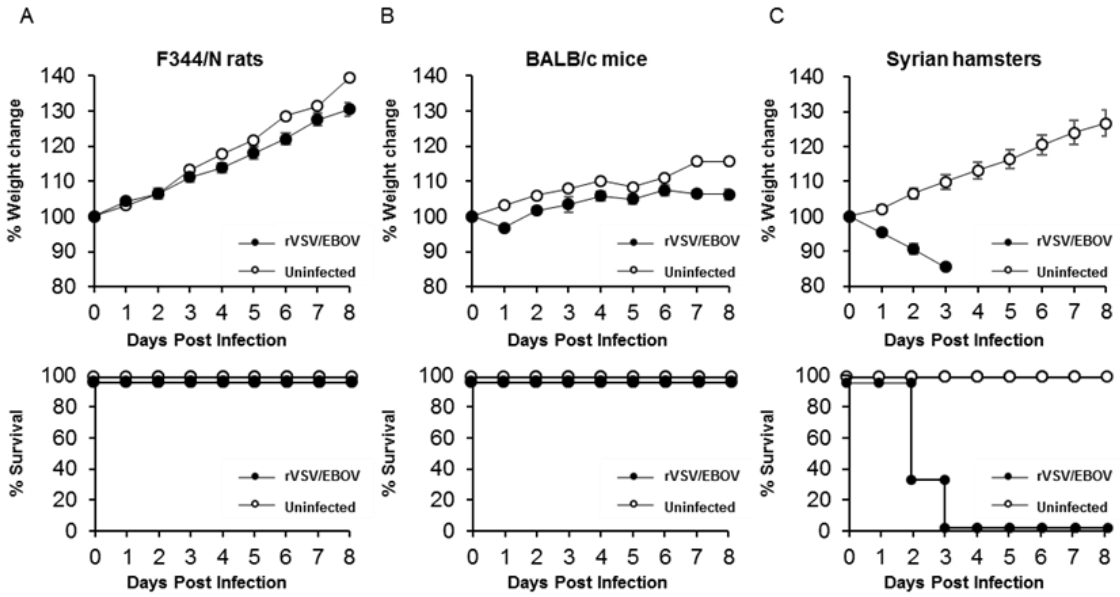

Figure 1. Body weight changes and survival curves of animals after rVSV/EBOV infection. (A) F344/N rats, (B) BALB/c mice, and (C) Syrian hamsters (3 animals for each group) were injected intraperitoneally (i.p.) with 10^7, $10^{6.5}$, and $10^{7.2}$ PFU of rVSV/EBOV, respectively. The symbols represent mean group weights and the bars represent standard errors.

Lethal Infection with Recombinant VSVs in Syrian Hamsters

To determine the LD_{50} of rVSV pseudotyped with the GP of EBOV or MARV (another human-pathogenic filovirus), Syrian hamsters were infected with rVSV/EBOV or rVSV/MARV. The parental VSV (rVSV/VSV) was also tested to determine its pathogenicity in hamsters. Three or four groups of hamsters were infected i.p. with serially diluted rVSV/EBOV, rVSV/MARV, or rVSV/VSV and their body weight loss was monitored. I found that all these viruses induced body weight loss and fatal outcomes (Figure 2). Among rVSV/EBOV-infected hamsters (Figure 2A), animals infected with 10^6 PFU of the virus showed the most severe body weight loss and all of them succumbed within 5 dpi. The severity of body weight reduction was virus dose-dependent and the calculated LD_{50} value was $10^{4.8}$ PFU. All hamsters infected with rVSV/MARV also showed a significant body weight loss in a virus dose-dependent manner (Figure 2B). Two of three animals infected with $10^{6.5}$ and $10^{7.5}$ PFU of rVSV/MARV succumbed within 4 dpi. (LD_{50} = $10^{6.2}$ PFU) (Figure 2B). rVSV/VSV also caused severe and fatal diseases in hamsters as described previously [67,68], and the LD_{50} value of rVSV/VSV was lower ($10^{2.8}$ PFU) than those of rVSV/EBOV and rVSV/MARV (Figure 2C).

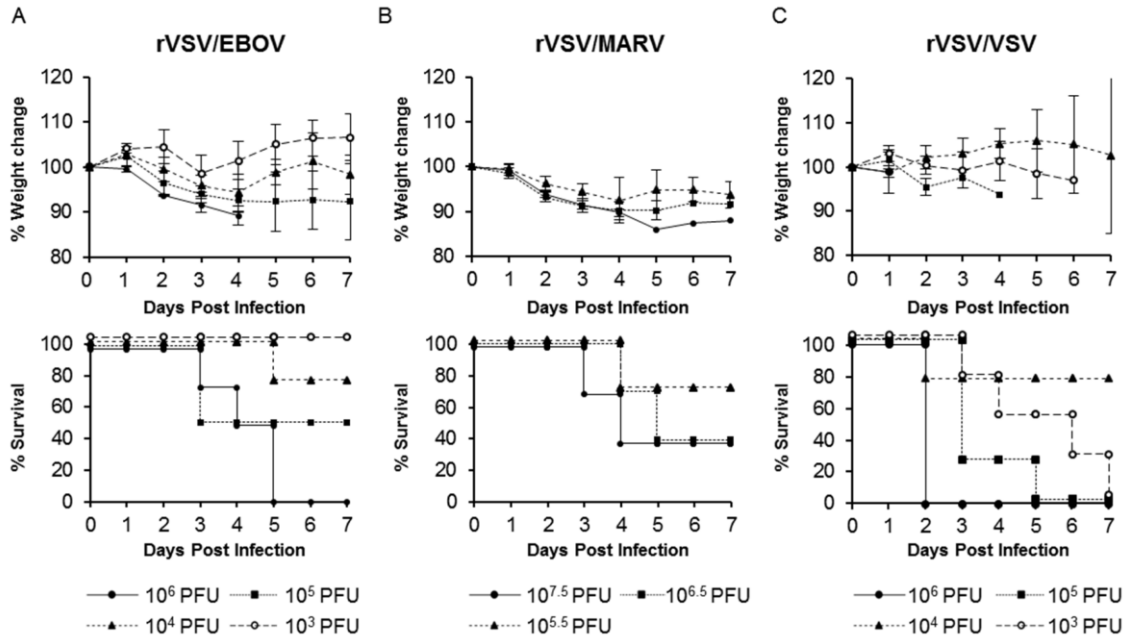

Figure 2. Body weight changes and survival curves of Syrian hamsters infected with rVSV/EBOV, rVSV/MARV, or rVSV/VSV. (A) Four hamsters were infected i.p. with 10^6, 10^5, 10^4, or 10^3 PFU of rVSV/EBOV. (B) Three hamsters were infected i.p. with $10^{7.5}$, $10^{6.5}$, or $10^{5.5}$ PFU of rVSV/MARV. (C) Four hamsters were infected i.p. with 10^6, 10^5, 10^4, or 10^3 PFU of rVSV/VSV. All animals were monitored for body weight and survival for 7 days post-infection (dpi). The symbols represent mean group weights and the bars represent standard errors (A, B, and C upper panel).

Virus Dissemination and Pathological Change in Recombinant VSV-Infected Syrian Hamsters

I then investigated viral replication in hamsters (Figure 3). Three groups of four Syrian hamsters were infected with rVSV/EBOV, rVSV/MARV, or rVSV/VSV and tissue samples (liver, spleen, kidney, heart, lung, brain, salivary gland, testis, and colon) were collected 36 hours after infection to determine viral titers (Figure 3) and to examine pathological changes (Figure 4). All the tested tissue samples had detectable viral titers and the mean viral loads ranged from $10^{4.30}$ to $10^{7.53}$, $10^{2.70}$ to $10^{7.45}$, and $10^{6.27}$ to $10^{8.88}$ PFU per gram of tissue for rVSV/EBOV, rVSV/MARV, and rVSV/VSV, respectively. In rVSV/EBOV-infected hamsters, the infectious virus was recovered from liver, spleen, lung, testis, and colon tissues at high titers and relatively lower titers of the virus were detected in the kidney, heart, brain, and salivary gland (Figure 3A). The viral load in brain tissue was the lowest ($10^{5.12}$ PFU/g). Similar trends were observed in rVSV/MARV-infected hamsters (Figure 3B). The virus titers in the brain were remarkably low ($10^{3.12}$ PFU/g). Compared with rVSV/EBOV and rVSV/MARV, viral titers of rVSV/VSV were overall higher in all the tissue samples, but the difference among tissues was less prominent (Figure 3C). These results indicated that rVSV/EBOV, rVSV/MARV, and rVSV/VSV caused systemic infection of hamsters.

Viral antigens were then investigated by IHC using the rabbit anti-VSV N polyclonal antibody (Figure 4A). In the liver, the viral antigen was detected in hepatocytes and capillary vessels along with severe hepatocellular necrosis and mild inflammation uniformly in rVSV/VSV-, rVSV/EBOV-, and rVSV/MARV-infected hamsters (Figure 4C). In the spleen, viral antigen-positive cells were mainly observed around white pulp in rVSV/EBOV- and rVSV/MARV-infected hamsters (Figure 4B and 4C). In rVSV/EBOV- and rVSV/MARV-infected hamsters, strong immunostaining of the viral antigen was seen in monocytic cells. In contrast, many cell types including monocytic cells and lymphocytes were viral antigen-positive in rVSV/VSV-infected animals (Figure 4B and 4C). In the brain, where rVSV/EBOV and rVSV/MARV replicated less efficiently than rVSV/VSV, the viral antigen distribution was different among the viruses; viral antigen-positive neurons were extensively observed in rVSV/VSV-infected hamsters and capillary vessels and neurons were weakly stained in rVSV/EBOV-infected hamsters (Figure 4A and 4C). Taken together, the IHC results were consistent with the viral loads in the organs and indicated that viral tropisms and primary target cells might vary among the viruses.

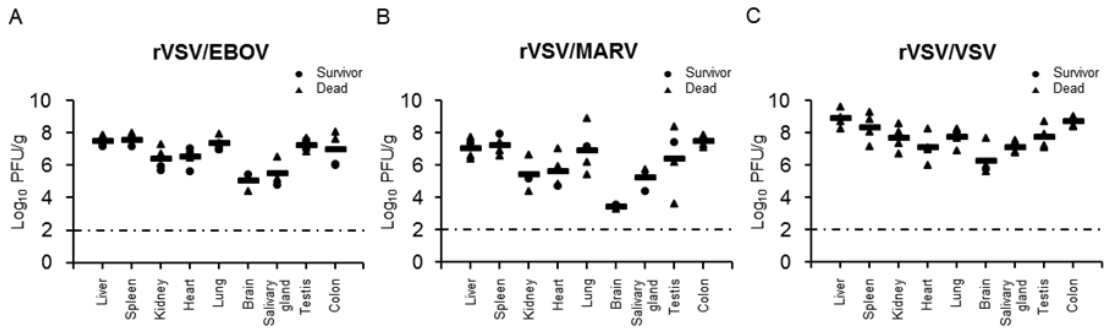

Figure 3. Virus titers in hamsters infected with rVSVs. Four hamsters in each group were infected i.p. with 10^7 PFU of (A) rVSV/EBOV, (B) rVSV/MARV, or (C) rVSV/VSV. Thirty-six hours after virus inoculation, tissue samples were collected and used for virus titration in plaque assays. Two of four rVSV/EBOV-infected, three of four rVSV/MARV-infected, and three of four rVSV/VSV-infected animals already succumbed at the sampling time point. Each symbol represents the value of an individual hamster. The bars represent the means for the infected hamsters. The broken lines indicate the detection limit (<2.0 log10 PFU/g).

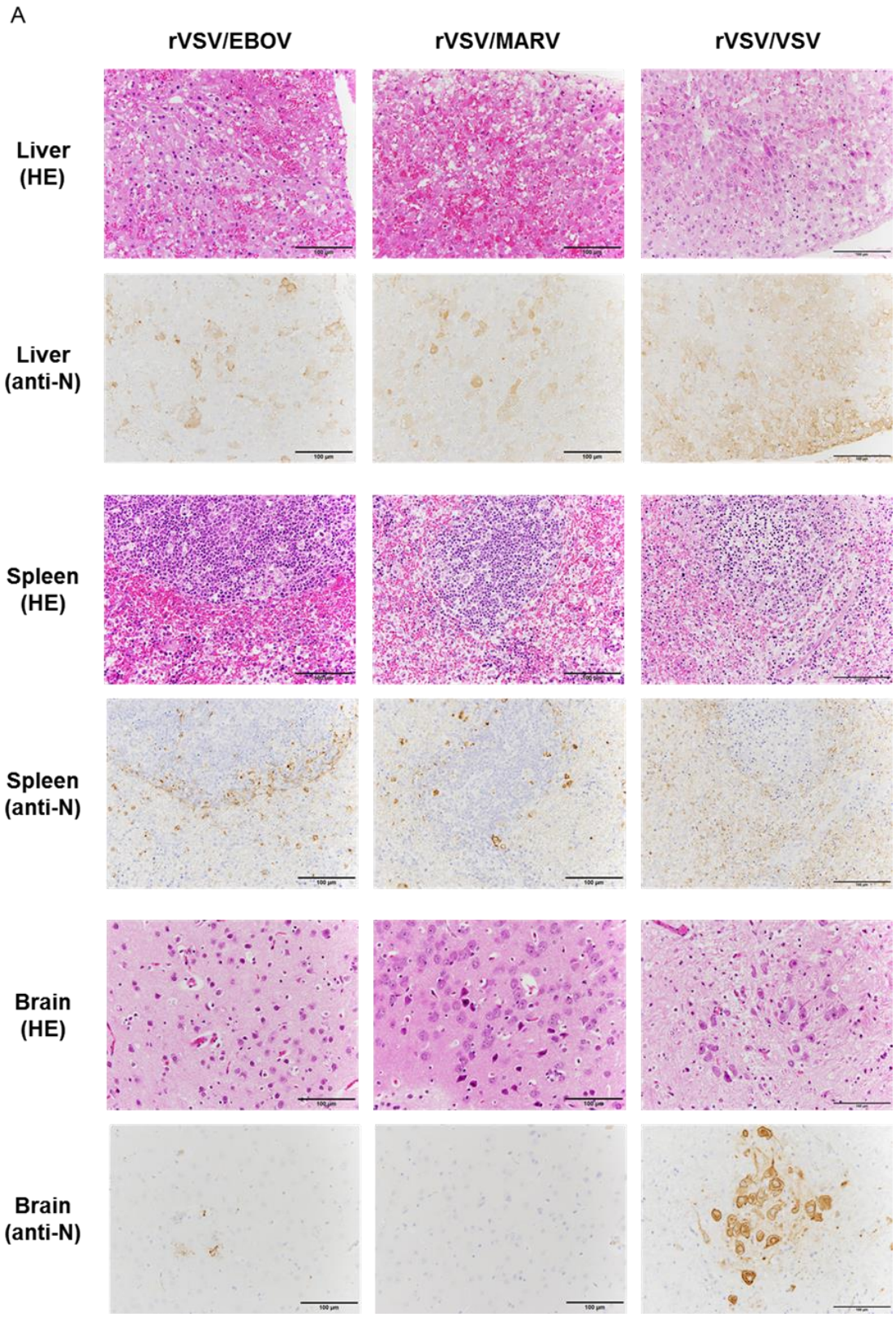
A
rVSV/EBOV
rVSV/MARV
rVSV/VSV
Liver (HE)
Liver (anti-N)
Spleen (HE)
Spleen (anti-N)
Brain (HE)
Brain (anti-N)

B

rVSV/EBOV

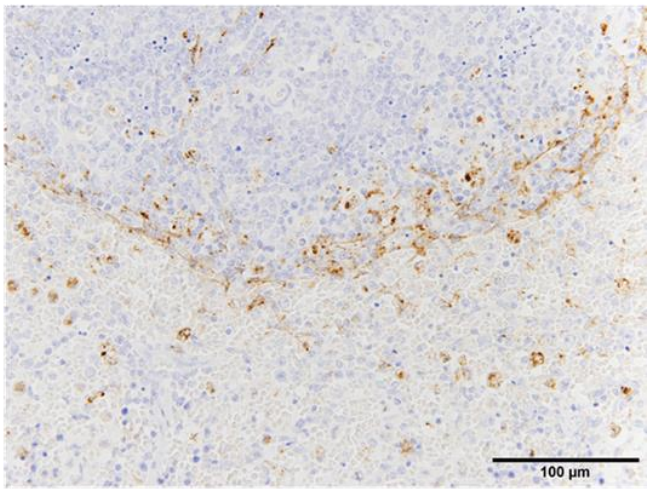

rVSV/MARV

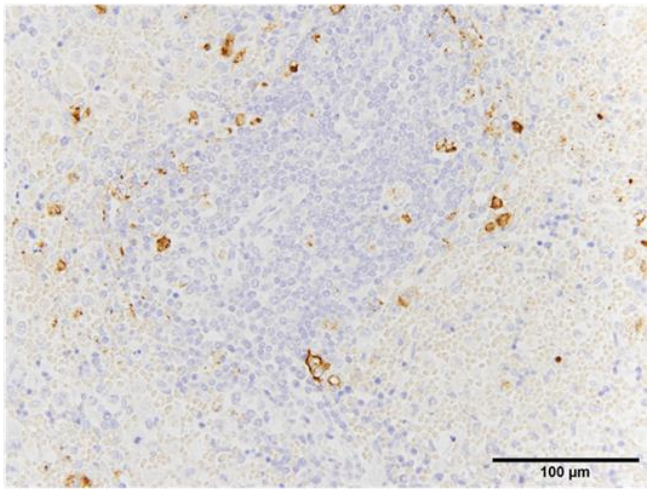

rVSV/VSV

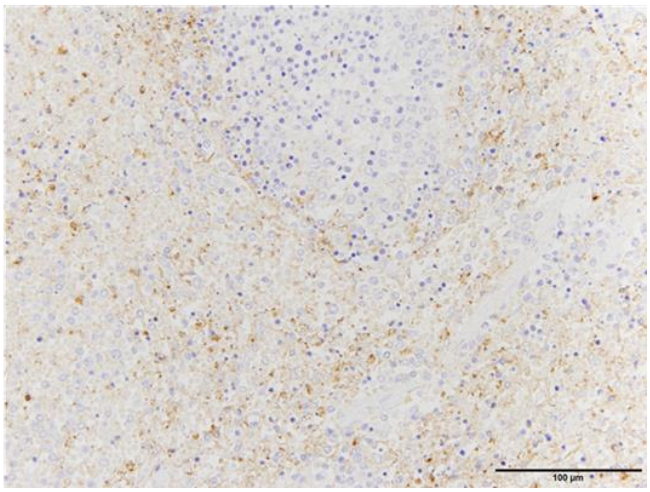

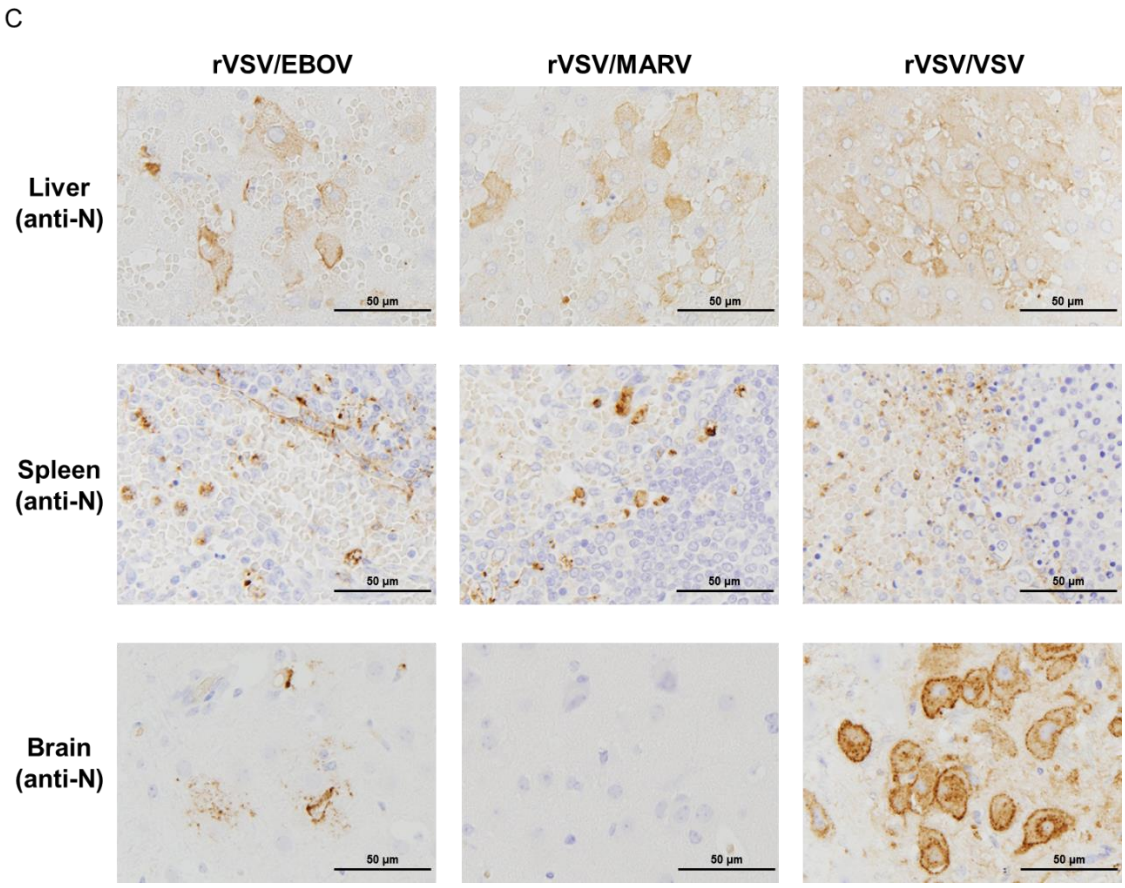

Figure 4. Histological and immunohistochemical analyses of liver, spleen, and brain (cerebral cortex). (A) Tissue sections were stained with hematoxylin and eosin (HE) and a rabbit anti-VSV N polyclonal antibody. Scale bars represent 100 μm. (B) Enlarged images of the spleen sections stained with the anti-VSV N antibody are also shown. Scale bars represent 100 μm. (C) High-power magnification images of the liver, the spleen, and the brain sections stained with the anti-VSV N antibody are also shown. Scale bars represent 50 μm. Brown-stained cells represent viral antigen-positive cells.

Hematology and Blood Biochemistry in Syrian Hamsters Infected with Recombinant VSVs

To investigate the hematologic and blood biochemical changes, animals infected with rVSV/EBOV, rVSV/MARV, and rVSV/VSV were euthanized 12 hours after infection and blood samples were collected for analysis. The results showed differences in the WBC, PLT, and LYM counts among rVSV/EBOV-, rVSV/MARV-, and rVSV/VSV-infected hamsters (Figure 5A). The numbers of WBC and LYM decreased upon infection in all the infected hamsters, although a significant difference was only found in rVSV/MARV-infected animals. Interestingly, a significant reduction of the PLT count in rVSV/EBOV-infected hamsters was observed. Although this effect was slightly seen in rVSV/MARV- and rVSV/VSV-infected animals, it was not significant compared to uninfected animals. Significant upregulation of liver parameters, AST and ALP, were observed in rVSV/EBOV- and rVSV/VSV-infected hamsters (Figure 5B). ALT was slightly, but not significantly, increased in rVSV/EBOV- and rVSV/VSV-infected hamsters. These results suggested that viral pathogenesis might differ among rVSV/EBOV, rVSV/MARV, and rVSV/VSV.

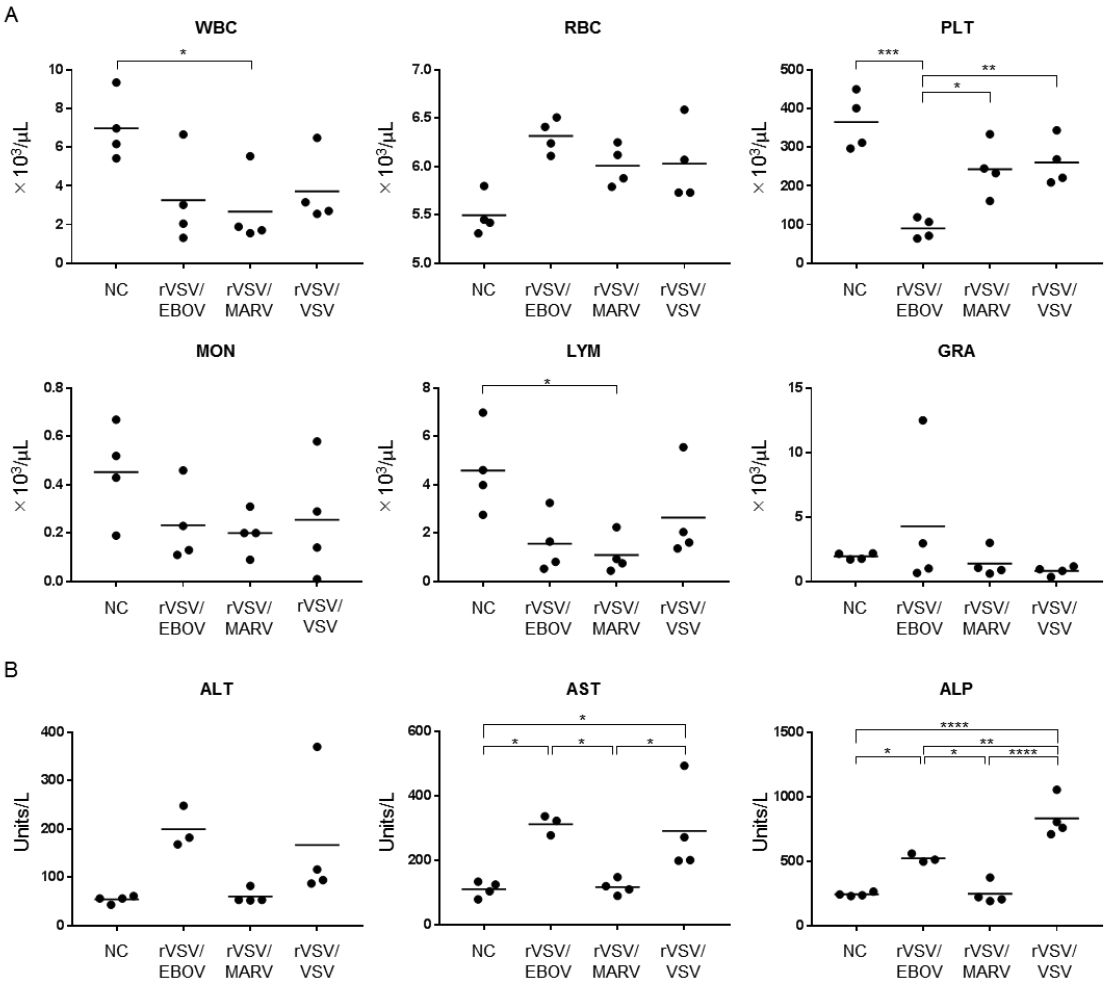

Figure 5. (A) Blood cell counts and (B) liver parameters in hamsters infected with rVSVs. Four hamsters in each group were infected i.p. with 10^7 PFU of rVSV/EBOV, rVSV/MARV, or rVSV/VSV. Twelve hours after virus inoculation, blood and serum samples were collected and used for cell counts and blood biochemistry. Each symbol represents the value for an individual hamster. The bars represent the means of the infected hamsters. * $P < 0.05$, ** $P < 0.005$, *** $P < 0.0005$, **** $P < 0.00005$.

Prophylactic and Therapeutic Effects of Antibody Treatment of Syrian Hamsters Infected with rVSV/EBOV

To test the utility of rVSV/EBOV-infected Syrian hamsters for *in vivo* screening of anti-EVD drugs, the prophylactic and therapeutic effects of passive immunization with an anti-EBOV GP-neutralizing MAb were investigated in this model. I used a human-mouse chimeric MAb (ch6D6) generated based on the variable region sequence of mouse MAb 6D6, which has been shown to provide high levels of protection against EBOV infection in mice [65,69]. Syrian hamsters were treated with 100 μg of MAb ch6D6 or chDNP (negative control MAb), one day before (Figure 6) or one hour after (Figure 7) the challenge with rVSV/EBOV, rVSV/MARV, or rVSV/VSV and their body weight changes and survival rates were monitored. The prophylactic treatment of animals with ch6D6 protected all three animals from lethal rVSV/EBOV infection, though one animal showed body weight loss. In contrast, all three animals that received chDNP showed body weight loss and one of them died at 2 dpi. As expected, the treatment of animals with ch6D6 did not show protective effects against rVSV/MARV and rVSV/VSV infection. The post-exposure therapeutic effect was also confirmed in this model (Figure 7). All animals treated with ch6D6 one hour after the virus challenge survived without body weight loss, whereas all of the chDNP-treated animals succumbed at 2 dpi. Infection of animals with rVSV/MARV and rVSV/VSV induced severe disease signs with remarkable weight loss regardless of the treatment and most of them succumbed at 2 or 3 dpi.

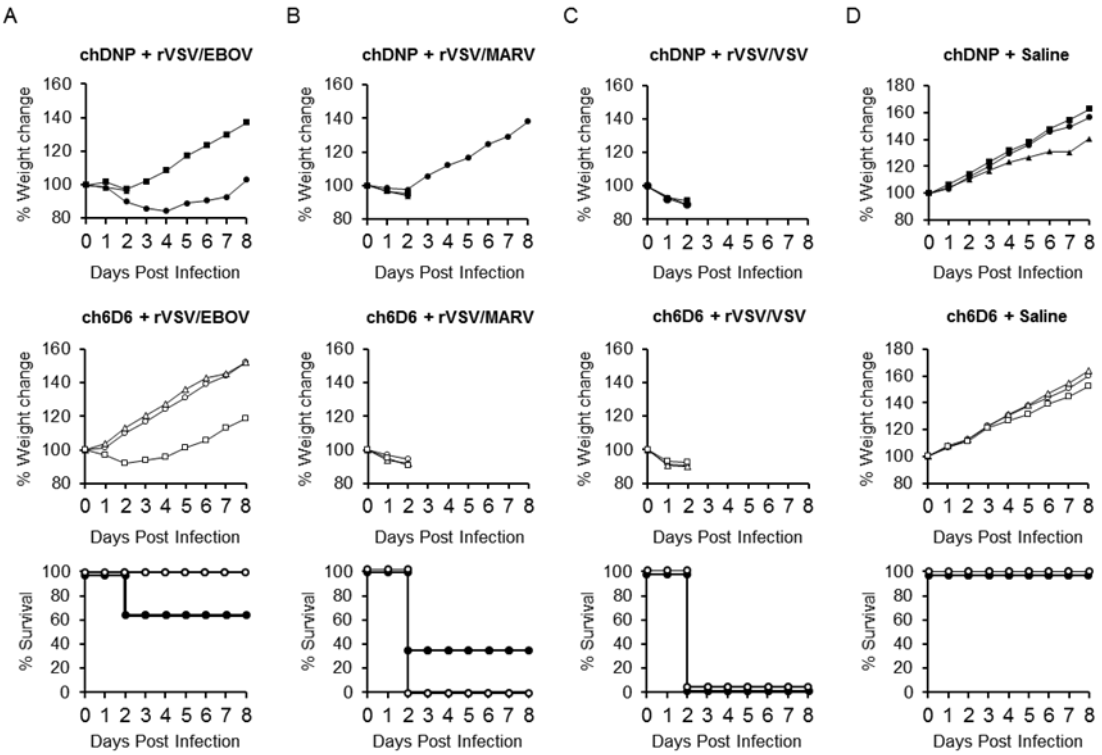

Figure 6. Effects of prophylactic treatment with the neutralizing antibody in rVSV/EBOV-infected hamsters. Three hamsters in each group were treated i.p. with 100 μg of MAb ch6D6 or negative control MAb chDNP one day before (A) rVSV/EBOV, (B) rVSV/MARV, or (C) rVSV/VSV i.p. challenge (10^7 PFU), or (D) treated with saline alone. Symbols represent percentages of body weight for each hamster (upper and middle panels). Open and solid symbols represent survival curves of 6D6- and chDNP-treated animals, respectively (lower panel).

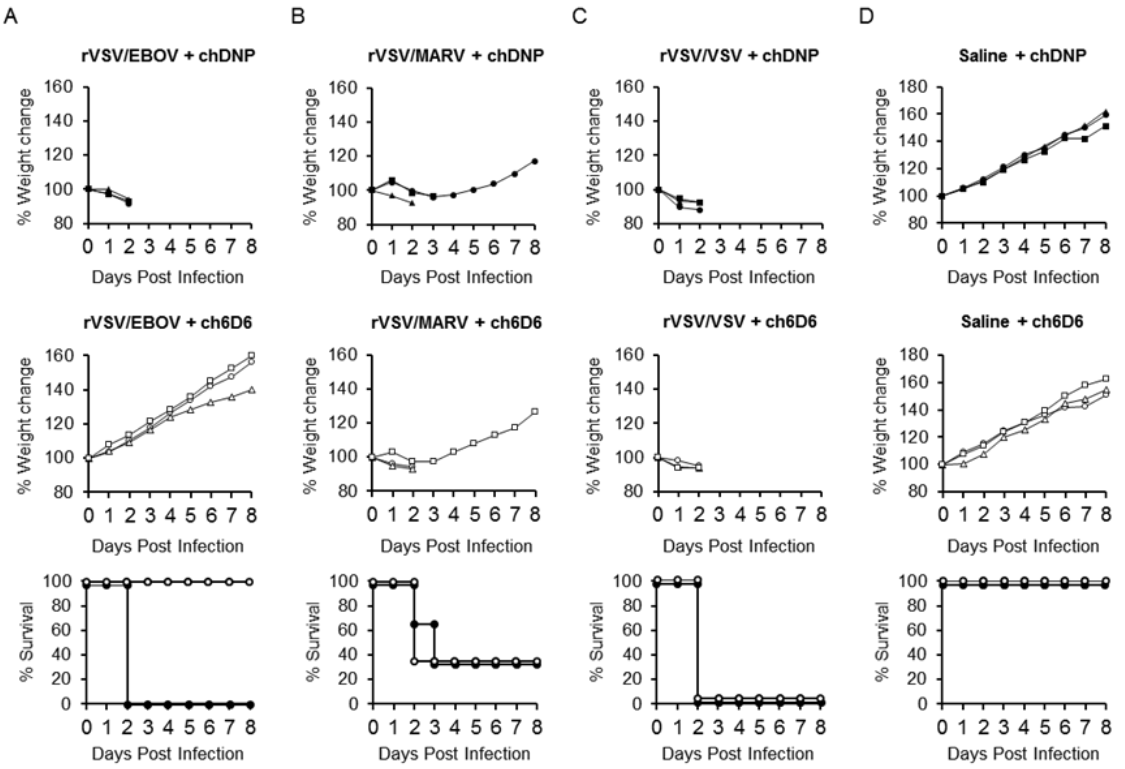

Figure 7. Therapeutic effect of post-exposure treatment with the neutralizing antibody in rVSV/EBOV-infected hamsters. Three hamsters in each group were treated i.p. with 100 μg of MAb ch6D6 or negative control MAb chDNP one hour after (A) rVSV/EBOV, (B) rVSV/MARV, or (C) rVSV/VSV i.p. challenge (10^7 PFU), or (D) treated with saline alone. Symbols represent percentages of weight for each hamster (upper and middle panels). Open and solid symbols represent survival curves of 6D6- and chDNP-treated animals, respectively (lower panel).

Discussion

In this study, I investigated the pathogenic potential of rVSV/EBOV and rVSV/MARV in mice, rats, and hamsters and evaluated the hamster model as an *in vivo* GP-targeting drug screening tool that could be handled under BSL-2 conditions. Rats and mice inoculated with high titers of rVSV/EBOV did not show body weight loss and infectious virus was not recovered from any of the tested tissues collected at 2 dpi (data not shown). However, GP-specific serum IgG antibodies were detected at high titers in all of the animals at the end of each experiment (data not shown), indicating asymptomatic infection in rats and mice by rVSV/EBOV. In contrast, rVSV/EBOV infection resulted in fatal outcomes for Syrian hamsters. It was reported that rVSV/EBOV used as a live attenuated vaccine candidate induced strong immunity against EBOV GP and protected 6-week-old hamsters from lethal MA-EBOV infection [62]. In that study, the hamsters were inoculated with 10^5 PFU of rVSV/EBOV and systemic replication of rVSV/EBOV was confirmed at 1 dpi, but it is unclear whether these rVSV/EBOV-infected hamsters showed disease signs or not. In my study, hamsters infected with 10^5 PFU of rVSV/EBOV showed significant body weight loss and some of them succumbed within 2 dpi. Infection with a higher dose (10^7 PFU) of rVSV/EBOV also led to fatal outcomes and the virus was recovered from all the tested tissues, consistent with the previous study [62]. It is conceivable that the difference in susceptibility to VSV among hamster strains affected the different outcomes. Previous reports and my results indicate that WT VSV Indiana induces fatal infection of hamsters [67,68,70]. However, differential susceptibility among inbred Syrian hamster strains to the VSV Indiana serotype was reported [67,68]. The susceptibility of outbred Syrian hamsters to rVSV/EBOV might vary depending on their genetic backgrounds.

Interestingly, the tissue tropism of rVSV/EBOV and rVSV/MARV might differ from that of rVSV/VSV. In rVSV/VSV-infected animals, the virus was detected in all of the tested organs at high titers, suggesting the pantropicity of this virus. By contrast, rVSV/EBOV and rVSV/MARV seemed to prefer target organs such as the liver, spleen, and lung. The virus titers were much lower in the brain samples collected from rVSV/EBOV- and rVSV/MARV-infected hamsters than in those from rVSV/VSV-infected animals, which is consistent with the observation that the nervous system is not the main target of EBOV and MARV [8]. Importantly, the histopathological analysis of the infected animals also revealed different cellular tropisms among the viruses. It is noteworthy that rVSV/EBOV and rVSV/MARV, but not rVSV/VSV, preferentially infected monocytic cells in the spleen, which are known to be one of the major target cells of EBOV and MARV [14,15]. These observations suggest that rVSV/EBOV and

rVSV/MARV might have tissue tropisms similar to those seen in actual EBOV and MARV infection in mice and nonhuman primates. Since inflammation is most likely the key factor of pathology in most animal models and human cases of EBOV and MARV infections, the infection of macrophages and dendritic cells might also play important roles in the pathogenesis of this hamster model although the immune regulation mechanisms mediated by viral proteins other than GP should differ from those in animals infected with authentic EBOV and MARV.

Different viral tropisms are often determined by the interaction between viral envelope proteins and their host receptors. VSV exhibits a robust pantropic infectivity mediated by its envelope protein, VSV G. It has been reported that nonspecific electrostatic and hydrophobic interactions mediate the attachment of VSV to cells [71,72]. The involvement of the cell surface LDL receptor as the major ubiquitous VSV cellular receptor has also been suggested [71,72]. On the other hand, the filovirus GP-mediated attachment to host cells is believed to have tropism to cells expressing C-type lectins such as DC/L-SIGN, hMGL, and LSECtin [14,15]. Hepatocytes, endothelial cells, dendritic cells, monocytes, and macrophages, all of which express C-type lectins, are thought to be preferred target cells of EBOV and MARV. In this study, I found that rVSV/EBOV and rVSV/MARV infected hepatocytes and monocytic cells, although tropism to endothelial cells was not clearly observed. In contrast, rVSV/VSV widely infected many types of cells, including hepatocytes, macrophages, lymphocytes, and capillary cells. These results suggest that rVSV/EBOV and rVSV/MARV preferentially infect particular types of cells, which is reflected by GP-mediated cell tropism, likely through the interaction with C-type lectins.

Patients having EVD or MVD typically present with abnormally low numbers of leukocytes, lymphocytes, and platelets at the time of clinical onset [73,74]. In all rVSV-infected animals, leukocytopenia and lymphocytopenia were observed and the degree was most severe in rVSV/MARV-infected hamsters. Interestingly, severe thrombocytopenia was only observed in rVSV/EBOV-infected hamsters. The coagulopathic state seen in EVD appears to be caused by a combination of activation of the mononuclear phagocytic system, platelet aggregation, and consumption [12,73,74]. My data suggest that rVSV/EBOV-infected hamsters might share a similar pathological mechanism with EBOV infection of humans and nonhuman primates, though rVSV/MARV seemed to have lower preference for the mononuclear phagocytic system.

Significant increases of ALT and AST and a high AST/ALT ratio are common features of EVD and MVD, indicating acute hepatic failure [73,74]. In the present study, elevated levels of serum liver enzymes were observed in rVSV/EBOV-infected hamsters,

but not in rVSV/MARV. I assumed that rVSV/EBOV induced pathological changes similar to those in actual EBOV infection of humans and NHPs, whereas rVSV/MARV caused milder infection in hamsters, resulting in less prominent pathological changes. The increase of the liver enzymes was also seen in rVSV/VSV-hamsters. Considering the pantropic property of VSV, elevated levels of the enzymes in rVSV/VSV-infected hamsters, particularly ALP levels that were higher than in rVSV/EBOV-infected animals, might suggest that rVSV/VSV induced severe multiple organ disfunction that was distinct from that observed in rVSV/EBOV- and rVSV/MARV-infected animals.

In the present study, I confirmed the pathogenicity of replication-competent rVSV pseudotyped with filovirus GPs in Syrian hamsters, and demonstrated the utility of this model to investigate the prophylactic and therapeutic effects of passive immunization with an anti-GP neutralizing antibody. Since the entry of rVSV/EBOV and rVSV/MARV into target cells depends on the function of GPs, this animal model is a useful tool for screening of anti-GP drugs under BSL-2 conditions and is expected to accelerate drug development targeting the function of GPs.

Summary

The development of vaccines or antivirals against EVD and MVD have been hampered because of biosafety restriction of EBOV and MARV. To accelerate the development of countermeasures against these diseases, it is necessary to generate the surrogate model that can be conducted under BSL-2 or -3 facilities. I investigated the susceptibilities to rVSV/EBOV among experimental animals including mice, rat, and Syrian hamsters, and only hamster showed lethal outcomes. The pathogenicity of rVSV/EBOV or rVSV/MARV to hamsters shared some features with EBOV or MARV infection in humans such as severe hepatocellular necrosis, resemble tissue and cell tropisms including hepatocytes or monocytes and depletion of the number of platelets that did not observed in rVSV/VSV infection animals. This observation suggested that the pathogenicities and cellular tropisms of rVSV/EBOV and rVSV/MARV were mainly determined by their surface glycoprotein derived from EBOV and MARV. Using this model, I confirmed the therapeutic effect of passive immunization with the anti-EBOV monoclonal antibody targeting EBOV GP before/after virus inoculation. From this result, this animal model seems to be attractive *in vivo* GP-targeting drug screening tool that could be handled under BSL-2 conditions.

Chapter II:

Molecular mechanisms underlying the cellular entry and host range restriction of Lujo virus, an arenavirus

Introduction

Viruses in the family *Arenaviridae* are divided into four genera: *Antennavirus*, *Hartmanivirus*, *Reptarenavirus*, and *Mammarenavirus*. The genus *Mammarenavirus* is classified into two major groups, the Old World (OW) and the New World (NW) arenaviruses, based on their serologic, genetic, and geographic relationships. Some mammarenaviruses infect humans and cause diseases ranging from asymptomatic to severe hemorrhagic fever. Of these, LASV and LUJV, OW arenaviruses, are etiologic agents of fatal hemorrhagic fevers in humans. NW arenaviruses, including Junin, Machupo, Sabia, Guanarito, and Chapare viruses, are also known to cause hemorrhagic fevers in humans [9,10]. LUJV caused an outbreak in 2008 in Zambia and South Africa. Although the number of patients was limited, the mortality rate reached 80% [10,11]. In general, rodents are natural reservoirs of arenaviruses, except for Tacaribe virus isolated from an artibeus bat [9,75]. A natal multimammate mouse (*Mastomys natalensis*) is known as the natural host of LASV; however, the reservoirs of LUJV are still unknown [76,77]. To establish effective countermeasures against arenavirus infections, it is important to understand the molecular bases on their pathogenicities and host ranges.

Arenaviruses are enveloped, two-segmented single-stranded ambisense RNA viruses. The S segment of the viral genome encodes the glycoprotein (GP) precursor and the nucleoprotein and the L segment encodes the matrix protein (Z) and the RNA-dependent RNA polymerase (L) [9,13]. GP is synthesized as a single polypeptide chain and cleaved post-translationally into mature GP1 and GP2 by a cellular proprotein convertase, subtilisin kexin isozyme-1/site-1 protease [78,79]. GP1 is located on the top of the viral surface GP spike and mediates the attachment of virions to the target cell. GP2 contains the transmembrane region of the GP spike and mediates membrane fusion between the viral envelope and host cell membrane [13,18]. In accordance with the phylogenetic differences of GP sequences, arenaviruses utilize different cellular receptors. It is known that NW and OW arenaviruses use human transferrin receptor-1 (TfR1) and α-dystroglycan (α-DG), respectively [13,18]. On the other hand, NRP2 and CD63 have been reported as the cellular factors for LUJV infection [16]. NRP2 acts as the attachment receptor and the direct interaction between LUJV GP1 and NRP2 has been well investigated [16,17]. CD63 is thought to be required for pH-activated GP-mediated

membrane fusion in endosomes. However, the detailed mechanisms by which the interaction between CD63 and LUJV GP triggers membrane fusion is still unclear [16].

Although LUJV causes severe and life-threatening hemorrhagic fevers in humans, previous reports suggested different susceptibilities to LUJV infection among animal species. Cynomolgus macaques experimentally infected with LUJV only displayed mild, non-lethal illness [34]. More prominent differences in the susceptibility to LUJV were reported among rodents. LUJV did not cause any clinical symptoms or mortality in newborn and weanling mice, whereas LUJV-infected guinea pigs developed hemorrhagic manifestations similar to the symptoms observed in human cases [35]. However, neither viral nor cellular factors that explain such differential susceptibility among animal species have been elucidated.

To determine the molecular mechanisms underlying the potential host specificity of LUJV, I focused on the difference between human and rodent CD63 proteins. Using replication-incompetent VSV pseudotyped wtih LUJV GP (VSVΔG-LUJV/GP) [36], I found rodent-derived cell lines that showed significantly lower susceptibility than the human derived-cell lines tested and further demonstrated that a single amino acid residue located in the large extracellular loop (LEL) [16–18] was essential for the differential susceptibility to VSVΔG-LUJV/GP. It is suggested that the importance of the interaction of LUJV GP with the LEL region of CD63 for LUJV infection and also provide useful information for understanding the molecular basis of the host range of LUJV.

Materials and methods

Cell lines

African green monkey kidney Vero E6, human embryonic kidney HEK293T, human hepatoma Huh7, murine embryo fibroblast NIH3T3, and baby hamster kidney fibroblast BHK cells were grown in DMEM (Sigma) supplemented with 10% FCS (Cell Culture Bioscience), 100 U/ml penicillin, and 0.1 mg/ml streptomycin (Gibco). Plat-GP cells (Cell Biolabs) were grown in DMEM supplemented with 10% FCS. All the cell lines were grown at 37°C in a 5% CO_2 incubator.

Viruses

VSV containing the green fluorescent protein (GFP) gene instead of the VSV glycoprotein (G) protein gene (VSVΔG-G) and pseudotyped VSVs bearing GPs of LASV (strain Josiah) or LUJV (strain IGR140) were generated as described previously [36,80,81]. Infectious units (IU) of the pseudotyped VSVs in each cell line were determined as described previously [65,82]. Briefly, cells were seeded in 96-well plates one day before virus inoculation and 24 hours later GFP-positive cells were counted using an IN Cell Analyzer 2000 (GE Healthcare). To reduce the background infectivity of the residual parent VSVΔG-G, each pseudotyped virus stock was treated with a neutralizing monoclonal antibody specific to VSV G protein (VSV-G[N]1-9) before use [83]. The use of VSVs was approved by the Committee for Safety Management of Pathogens, Research Center for Zoonosis Control, Hokkaido University (10[06]) and Hokkaido University Safety Committee for Genetic Recombination Experiments (21[4]).

Construction of plasmids and generation of cells expressing CD63 and/or NRP2

Total RNA was extracted from HEK293T, NIH3T3, and BHK cells using ISOGEN (Nippongene) and mRNAs were reverse transcribed with Superscript IV (Invitrogen). To amplify the CD63 and NRP2 genes, polymerase chain reaction (PCR) was performed with KOD-One (TOYOBO) using primer sets designed based on the sequences of human CD63 (Genbank accession number; NM_001257389.1), mouse CD63 (Genebank accession number; NM_001042580.1), hamster CD63 (Genbank accession number; XM_013120354.2), and human NRP2 (Genbank accession number; NM_201266.1). The cDNA encoding human CD63 fused with an N-terminal 3×FLAG tag was cloned into the pMXs-neo vector (Cell Biolabs) using an In-Fusion cloning kit (BD Clontech) and the cDNA encoding human NRP2 fused with a C-terminal HA (hemagglutinin) tag was also cloned into the pMXs-puro vector (Cell Biolabs). In the same way, the cDNAs encoding mouse CD63 and hamster CD63 were also cloned into

the pMXs-neo vector. The cDNA encoding chimeric CD63 and point mutant CD63 were amplified using KOD-One and the primers containing the desired mutations, and cloned into the pMXs-neo vectors using an In-Fusion HD Cloning Kit (Clontech). To generate the retroviruses carrying the CD63 or NRP2 genes, Plat-GP cells were transfected with the pMXs-neo or pMXs-puro vectors encoding cDNA of these genes together with the expression plasmid pCAGGS encoding the VSV G gene using the TransIT-LT1 transfection reagent (Mirus) according to the manufacturer's instructions. Two days after transfection, the culture supernatants were collected, filtrated with 0.45-μm filters, and inoculated into BHK cells. BHK cells stably expressing CD63 or NRP2 were selected with DMEM containing 10% FCS and 1,000 μg/ml G418 (GE Healthcare) or 10 μg/ml puromycin (InvivoGen). BHK cells stably expressing both human CD63 and NRP2 were generated by infecting BHK cells with both retroviruses carrying human CD63 and NRP2, and selected with both 1,000 μg/ml G418 and 10 μg/ml puromycin. The expression of exogenous CD63 and NPR2 was confirmed by western blotting analysis. For vector control cells, BHK cells were transduced with the retrovirus produced with the pMXs-neo vector alone. The use of recombinant plasmids was approved by Hokkaido University Safety Committee for Genetic Recombination Experiments (21[4]).

Sodium dodecyl sulfate-polyacrylamide gel electrophoresis (SDS-PAGE) and western blotting

Cells (6.0×10^5 cells for each cell line) were lysed with 100 μl RIPA buffer (50 mM Tris-HCl [pH 7.4], 150 mM NaCl, 1% NP-40, 0.5% sodium deoxycholate, and 0.1% SDS) containing a protease inhibitor mixture (Roche) and incubated for 30 min on ice. After centrifugation (10,000×g at 4°C) for 10 min, supernatants were mixed with SDS-PAGE sample buffer (Bio-Rad) containing 10% 2-mercaptoethanol and incubated for 5 min at 98°C. The lysed proteins were separated in 6% (for NRP2) or 10% (for CD63 and β actin) SDS-PAGE and transferred to a polyvinylidene fluoride (PVDF) membrane (Merck). PBS containing 5% skim milk (BD) and PBS containing 0.05% Tween 20 (PBST) were used as blocking and wash buffers, respectively. The PVDF membrane was incubated with a mouse anti-FLAG M2 monoclonal antibody (Sigma), goat anti-NRP2 polyclonal antibody (R&D), or mouse anti-β actin monoclonal antibody (Abcam) for 60 min, washed with PBST, and then incubated with a goat anti-mouse IgG polyclonal antibody conjugated with horseradish peroxidase (HRP) or donkey anti-goat IgG polyclonal antibody conjugated with HRP (Jackson ImmunoResearch) for 60 min. After washing with PBST, the bound antibodies were visualized with Immobilon Western (Millipore) and Amersham Imager 600 (GE Healthcare).

Immunofluorescence assay

To investigate the expression and localization of exogenous CD63, BHK cells expressing exogenous 3×FLAG-tagged CD63 were seeded into eight-well chamber slides (Merck) precoated with poly-L-lysine (Cultrex). At 24 hours after cell seeding, the cells were washed with ice-cold PBS, fixed and permeabilized with ice-cold methanol for 15 min. After washing with PBS, the cells were incubated with PBST containing 3% bovine serum albumin for blocking, followed by incubation with the mouse anti-FLAG M2 monoclonal antibody and a rat anti-lysosomal-associated membrane protein 1 (LAMP1) polyclonal antibody (Sigma) as a late endosome marker for 1 hour at room temperature. The cells were washed with PBST and then incubated with a goat Alexa Fluor 488-conjugated anti-mouse IgG antibody (Molecular Probes), goat Alexa Fluor 594-conjugated anti-rat IgG antibody (Molecular Probes), and 5 μg/ml Hoechst 33842 (Thermo Fisher) for 1 hour in the dark at room temperature. Images were acquired with a 100 × oil objective lens on a Zeiss LSM700 inverted microscope using ZEN 2009 software (Carl Zeiss).

Fusion assay

To increase the cell-surface localization of CD63 exogenously introduced into HEK293 cells, retroviruses expressing CD63 with a mutated C-terminal lysosomal targeting motif (GY234AA) [84] were generated and HEK293 cells were transduced with the viruses. The surface localization of the exogenous CD63 was confirmed by flow cytometric analysis. For this analysis, a mouse anti-human CD63 monoclonal antibody (FUJIFILM Wako Pure Chemical Corporation) and rat anti-mouse CD63 monoclonal antibody (MBL) as primary antibodies and a goat Alexa Fluor 488-conjugated anti-mouse IgG antibody (Molecular Probes) and goat Alexa Fluor 488-conjugated anti-rat IgG antibody (Molecular Probes) as secondary antibodies were used. As the target cells, 1.5×10^5 HEK293 cells were cultured in poly-l-lysine coated 96-well plates and, 6 hours later, the cells were transfected with pCAGGS encoding the LUJV GP gene and pTOPO-T7-IRES-nanoluciferase using TransIT-LT1 transfection reagent (Mirus) according to the manufacturer's instructions. The expression of surface LUJV GP was confirmed by flow cytometry using an in-house mouse anti-LUJV GP monoclonal antibody. As the effector cells, 3.0×10^5 HEK293 cells stably expressing exogenous CD63 were seeded in 6-well plates at 6 hours prior to transfection. As vector control cells, HEK293 cells transduced with the retrovirus produced with pMXs-neo vector were used. The effector HEK293 cells were transfected with pCAGGS plasmids encoding the GFP and pCAGGS-T7 polymerase genes using TransIT-LT1. Twenty-four hours after transfection, the effector

cells were harvested with trypsin-EDTA and resuspended in DMEM supplemented with 10% FCS, and then 3.0×10^4 cells were overlaid onto the target cells in each well of 96-well plates. After co-culturing target and effector cells for 24 hours, the cells were washed once with PBS and then treated with citrate-phosphate buffer (pH 4.5) or PBS (pH 7.4) for 10 min at 37°C followed by washing with PBS and replacement of the medium with DMEM containing 10% FCS. After 24-hour incubation, syncytium formation was examined by fluorescent microscopy and fusion activity was quantified by measuring relative luciferase activity using the Nano-Glo Luciferase Assay System (Promega) according to the manufacturer's instructions. The use of recombinant plasmids was approved by the Ministry of Education, Culture, Sports, Science, and Technology, Japan.

Statistical analysis

All data were analyzed using GraphPad Prism v6.0 software. For comparison of viral infectivity among CD63-transduced cell lines, I performed a one-way repeated-measures analysis of variance, followed by Dunnett's test. P values of less than 0.05 were considered statistically significant.

Results

Differential susceptibility of human- and rodent-derived cell lines to VSVΔG-LUJV/GP and effects of NRP2 and CD63 expression on the susceptibility of BHK cells

To analyze the susceptibilities of human and rodent cell lines to arenaviruses, Vero E6 (African green monkey kidney), HEK293T (human kidney), Huh7 (human liver), NIH3T3 (mouse embryo fibroblast), and BHK (hamster kidney) cells were infected with VSV bearing Lassa virus GP (VSVΔG-LASV/GP), Lujo virus GP (VSVΔG-LUJV/GP), and VSV G protein (VSVΔG-G) (Figure 8A). I found that, unlike the tropism of VSVΔG-G, VSVΔG-LASV/GP and VSVΔG-LUJV/GP similarly infected Vero E6, Huh7, and HEK293T cells more efficiently than NIH3T3 and BHK cells, and this tendency was particularly prominent for the VSVΔG-LUJV/GP infectivity. Interestingly, VSVΔG-LUJV/GP showed much lower infectious units (2-3 log lower) in NIH3T3 and BHK cells than VSVΔG-LASV/GP. Notably, BHK cells were almost nonpermissive to VSVΔG-LUJV/GP. I then assumed that the differential susceptibility was due to the differences of the LUJV receptor molecules (i.e., NRP2 and CD63). To confirm the roles of these receptor molecules, I generated BHK cell lines stably expressing exogenous human CD63 and/or NPR2, and examined their susceptibilities to VSVΔG-LUJV/GP (Figure 8B). As expected, the expression of these molecules in BHK cells significantly enhanced the infectivity of VSVΔG-LUJV/GP, whereas only marginal enhancement was observed for the expression of NPR2. Accordingly, the amino acid sequences of the N-terminal CUB1 domain of NRP2, which is critical for binding between NRP2 and LUJV GP1 [9,10], are well conserved among mammalian species and there are no amino acid differences that could explain the lower susceptibility of the rodent cell lines tested, suggesting the limited role in the differential susceptibility between the human and rodent cell lines (Figure 8C). I then focused on the CD63 molecule, and BHK cell lines expressing human, mouse and hamster CD63s were generated for comparison of their susceptibilities to VSVΔG-LUJV/GP and VSVΔG-LASV/G. I confirmed similar intracellular localization and expression levels of the exogenous CD63s by confocal microscopy and western blotting (Figure 9A and 9B). In contrast to VSVΔG-LASV/GP, which uniformly infected all these cell lines, VSVΔG-LUJV/GP showed significantly higher infectivity in human CD63-expressing cells than in the cells expressing mouse or hamster CD63 (Figure 9C).

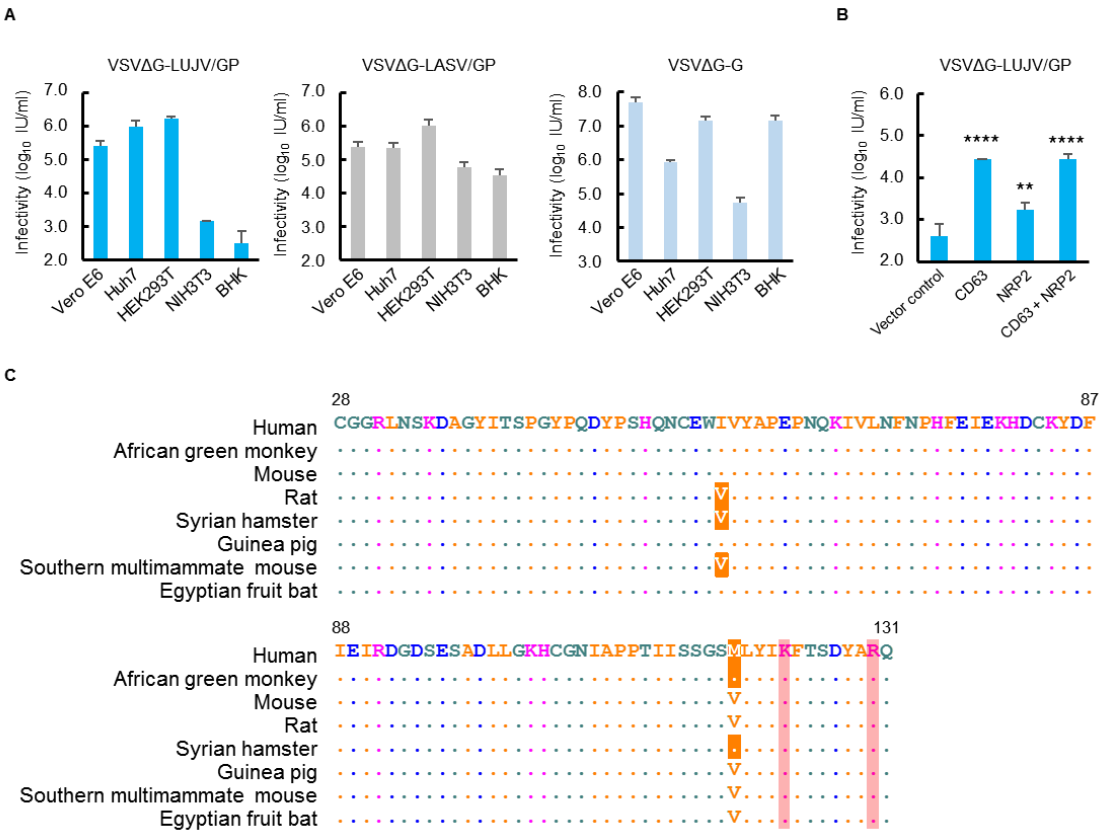

Figure 8. Differential susceptibility of primate- and rodent-derived cell lines to pseudotyped VSVs and importance of CD63 for LUJV entry into cells. (A) Infectious units (IU) of VSVΔG-LUJV/GP, VSVΔG-LASV/GP, and VSVΔG-G were determined in Vero E6, Huh7, HEK293T, NIH3T3, and BHK cells by counting the number of GFP-expressing cells as described in Materials and Methods. Each experiment was conducted three times, and averages and standard deviations are shown. (B) BHK cells transduced with exogenous human CD63 and/or NRP2 genes were infected with VSVΔG-LUJV/GP. The experiment was conducted three times, and averages and standard deviations are shown. Significant differences compared to the cells transduced with the vector control (Vector control) are shown (*P<0.05, **P<0.01, ***P<0.001, ****P<0.0001). (C) Amino acid sequences of the CUB1 region of NRP2 orthologs are aligned for the human (*Homo sapiens*; NP_003863.2), African green monkey (*Chlorocebus sabaeus*; XP_007964144.1), mouse (*Mus musculus*; NP_001070872.1), rat (*Rattus norvegicus*; XP_006245101.1), Syrian hamster (*Mesocricetus auratus*; XP_005070706.1), guinea pig (*Cavia porcellus*; XP_013012991.1), Southern multimammate mouse (*Mastomys coucha*; XP_031223558.1), and Egyptian fruit bat (*Rousettus aegyptiacus*; XP_015990573.1) in human NRP2 numbering. The amino acid residues directly interacting with LUJV GP1 (lysine and arginine at positions 123 and 130, respectively) are highlighted in pale red.

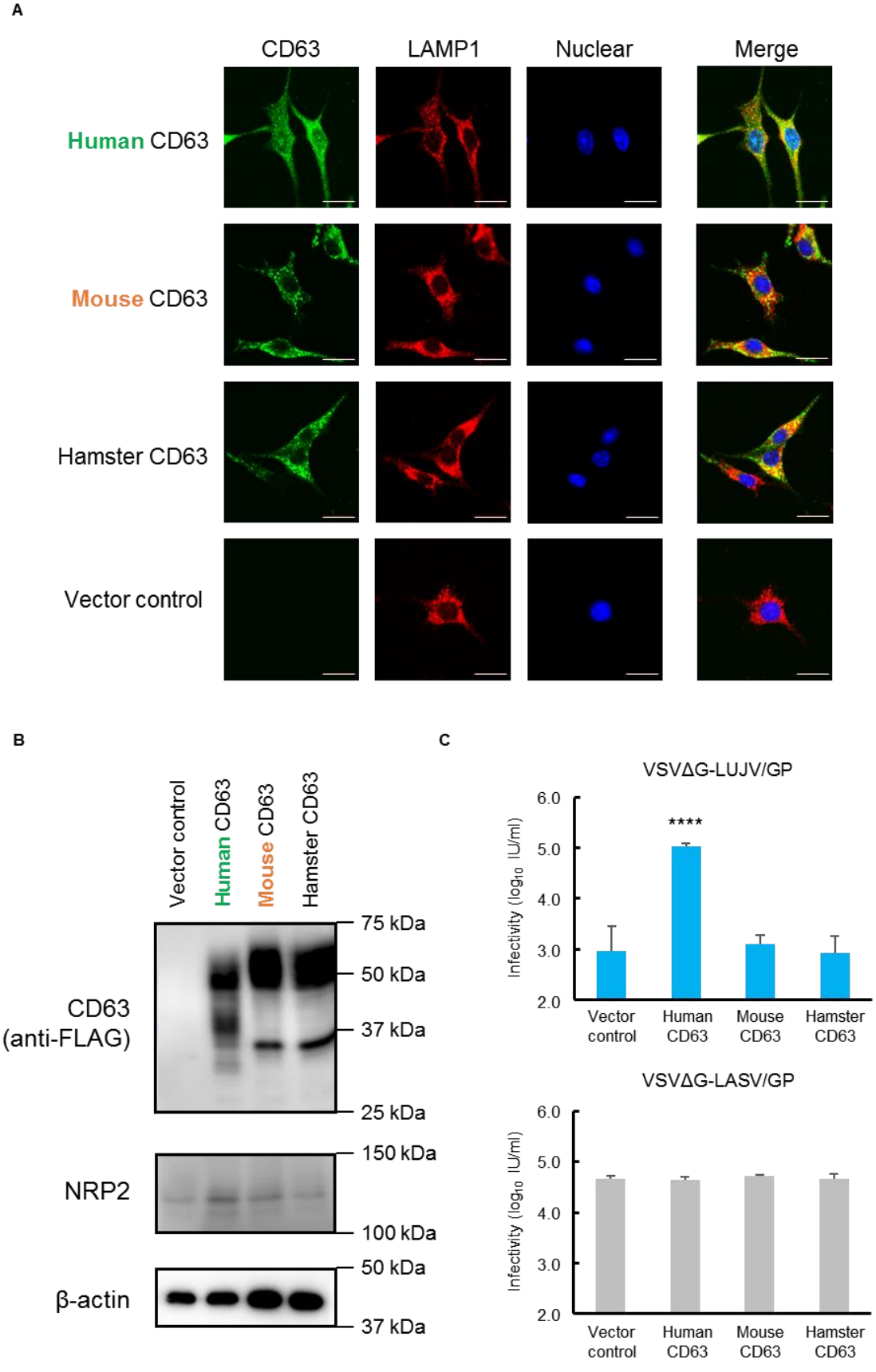
A
CD63
LAMP1
Nuclear
Merge
Human CD63
Mouse CD63
Hamster CD63
Vector control
B
Vector control
Human CD63
Mouse CD63
Hamster CD63
CD63 (anti-FLAG)
75 kDa
50 kDa
37 kDa
25 kDa
NRP2
150 kDa
100 kDa
β-actin
50 kDa
37 kDa
C
VSVΔG-LUJV/GP
Infectivity (log10 IU/ml)
6.0
5.0
4.0
3.0
2.0
****
Vector control
Human CD63
Mouse CD63
Hamster CD63
VSVΔG-LASV/GP
Infectivity (log10 IU/ml)
6.0
5.0
4.0
3.0
2.0
Vector control
Human CD63
Mouse CD63
Hamster CD63

Figure 9. Expression of exogenous human, mouse, and hamster CD63s in BHK cells and infectivities of VSVΔG-LUJV/GP and VSVΔG-LASV/GP. (A) The intracellular localization of exogenous CD63 in BHK cells was analyzed by confocal microscopy as described in Materials and Methods. The scale bars represent 20 μm. (B) Each cell lysate was separated in SDS-PAGE followed by western blotting as described in Materials and Methods. (C) Exogenous human, mouse, or hamster CD63-expressing BHK cells were infected with VSVΔG-LUJV/GP or VSVΔG-LASV/GP and infectious units (IU) were determined. Each experiment was conducted three times, and averages and standard deviations are shown. Significant differences compared to the cells transduced with the vector control (Vector control) are shown (*$P < 0.05$, **$P < 0.01$, ***$P < 0.001$, ****$P < 0.0001$).

Mapping of the functional regions in the CD63 molecule for VSVΔG-LUJV/GP infectivity

CD63 is a member of the tetraspanin family, which contains transmembrane (TM), N-terminal small extracellular loop (SEL), and C-terminal large extracellular loop (LEL) regions [85] (Figure 10A). Comparative sequence analysis of human and mouse CD63s revealed major differences located in the SEL and LEL regions (Figure 10B). To investigate which region of human CD63 is important for VSVΔG-LUJV/GP infection, I generated BHK cell lines stably expressing chimeric human-mouse CD63 proteins and compared their susceptibilities to the viruses (Figure 10C and 10D). The expression and the intracellular localization of the chimeric CD63s were confirmed by western blotting and confocal microscopy (Figure 11). Consistent with the results shown in Figure 9, all of the cell lines expressing human, mouse, or chimeric CD63 showed similar susceptibilities to VSVΔG-LASV/GP. In contrast, VSVΔG-LUJV/GP efficiently infected the cells expressing CD63 containing human CD63-derived LEL but not mouse CD63-derived LEL (Figure 10). The TM region of CD63 did not seem to make a major contribution to the infectivity of VSVΔG-LUJV/GP. These data indicated that the LEL region of human CD63 determined the high susceptibility of human cells to VSVΔG-LUJV/GP infection.

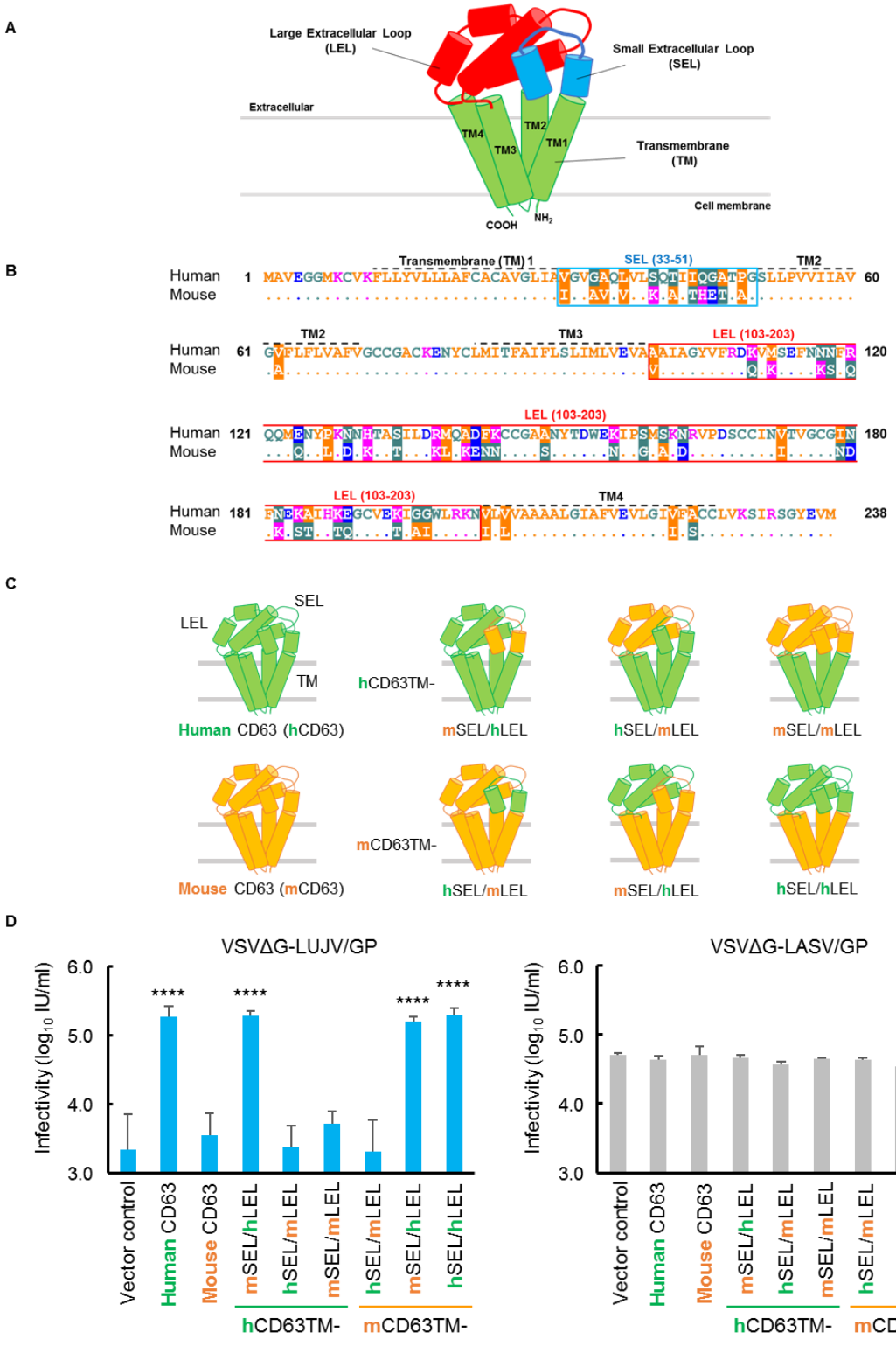
A
Large Extracellular Loop (LEL)
Small Extracellular Loop (SEL)
Extracellular
TM4
TM3
TM2
TM1
Transmembrane (TM)
Cell membrane
COOH
NH2
B
Transmembrane (TM) 1
SEL (33-51)
TM2
Human 1 MAVEGGMKCVKFLLYVLLLAFCACAVGLIAVGVGAQLVLSQTIIQGATPGSLLPVVIIAV 60
Mouse
TM2
TM3
LEL (103-203)
Human 61 GVFLFLVAFVGCCGACKENYCLMITFAIFLSLIMLVEVAAAIAGYVFRDKVMSEFNNNFR 120
Mouse
LEL (103-203)
Human 121 QQMENYPKNNHTASILDRMQADFKCCGAANYTDWEKIPSMSKNRVPDSCCINVTVGCGIN 180
Mouse
LEL (103-203)
TM4
Human 181 FNEKAIHKEGCVEKIGGWLRKNVLVVAAAALGIAFVEVLGIVFACCLVKSIRSGYEVM 238
Mouse
C
LEL
SEL
TM
Human CD63 (hCD63)
hCD63TM-
mSEL/hLEL
hSEL/mLEL
mSEL/mLEL
Mouse CD63 (mCD63)
mCD63TM-
hSEL/mLEL
mSEL/hLEL
hSEL/hLEL
D
VSVΔG-LUJV/GP
Infectivity (log10 IU/ml)
6.0
5.0
4.0
3.0
****
Vector control
Human CD63
Mouse CD63
mSEL/hLEL
hSEL/mLEL
mSEL/mLEL
hSEL/mLEL
mSEL/hLEL
hSEL/hLEL
hCD63TM-
mCD63TM-
VSVΔG-LASV/GP

Figure 10. Importance of the large extracellular loop (LEL) region of human CD63 for VSVΔG-LUJV/GP entry. (A) Schematic diagram of CD63. CD63 contains four transmembrane helixes (TM1-TM4), an N-terminal small extracellular loop (SEL), and a C-terminal large extracellular loop. (B) Comparison of amino acid sequences of human CD63 (NP_001244318.1) and mouse CD63 (NP_001036045.1). Amino acid residues different in human and mouse CD63s are highlighted. (C) Schematic diagram of chimeric CD63s produced in this study. The green and yellow colors indicate the regions derived from human and mouse CD63s, respectively. These chimeric CD63 proteins contain the human CD63 transmembrane domain (hCD63TM) or mouse CD63 transmembrane domain (mCD63TM). (D) BHK cells expressing wildtype human, mouse, and chimeric CD63s were infected with VSVΔG-LUJV/GP or VSVΔG-LASV/GP. The infectious units (IU) were determined as described in Materials and Methods. Each experiment was conducted three times, and averages and standard deviations are shown. Significant differences compared to the cells transduced with the vector control (Vector control) are shown (*$P < 0.05$, **$P < 0.01$, ***$P < 0.001$, ****$P < 0.0001$).

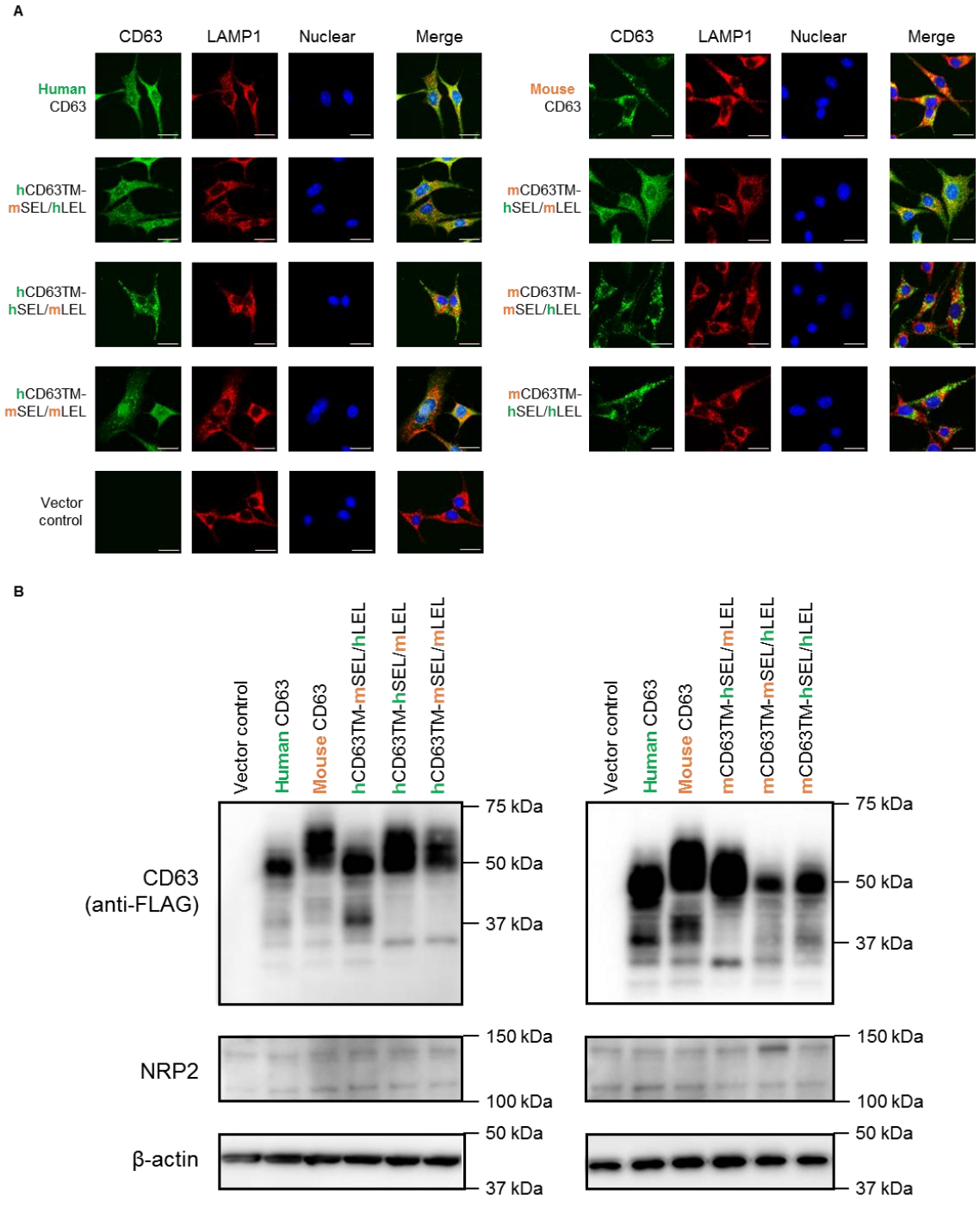

Figure 11. Expression of exogenous human and mouse CD63s and their chimeric mutants in BHK cells. (A) The intracellular localization of exogenous chimeric CD63 in BHK cells was analyzed by confocal microscopy as described in Materials and Methods. The scale bars represent 20 μm. (B) Each cell lysate was separated in SDS-PAGE followed by western blotting as described in Materials and Methods.

Contribution of amino acid residues at positions 141-150 in CD63 to VSVΔG-LUJV/GP infection

To determine the LEL region important for VSVΔG-LUJV/GP infection, I tested CD63 mutants having chimeric human-mouse CD63 LEL regions (Figure 12A). BHK cell lines stably expressing human and mouse WT CD63s and these CD63 mutants were infected with VSVΔG-LUJV/GP and VSVΔG-LASV/GP to compare their susceptibilities to the viruses (Figure 12B). The protein expression and intracellular localization were confirmed as described above (Figure 13). As expected, the expression of chimeric CD63 did not affect the susceptibility to VSVΔG-LASV/GP. In contrast, human CD63 having amino acid residues from mouse CD63 at positions 141-160 significantly decreased the ability to mediate VSVΔG-LUJV/GP entry and the replacement of this region in mouse CD63 with that of human LEL significantly increased the susceptibility of the cells. I further generated cells expressing chimeric CD63 in which the amino acid residues at positions 141-150 and 151-160 were swapped and found that the LEL region including amino acids at positions 141-150 was critical for VSVΔG-LUJV/GP infection (Figure 12B).

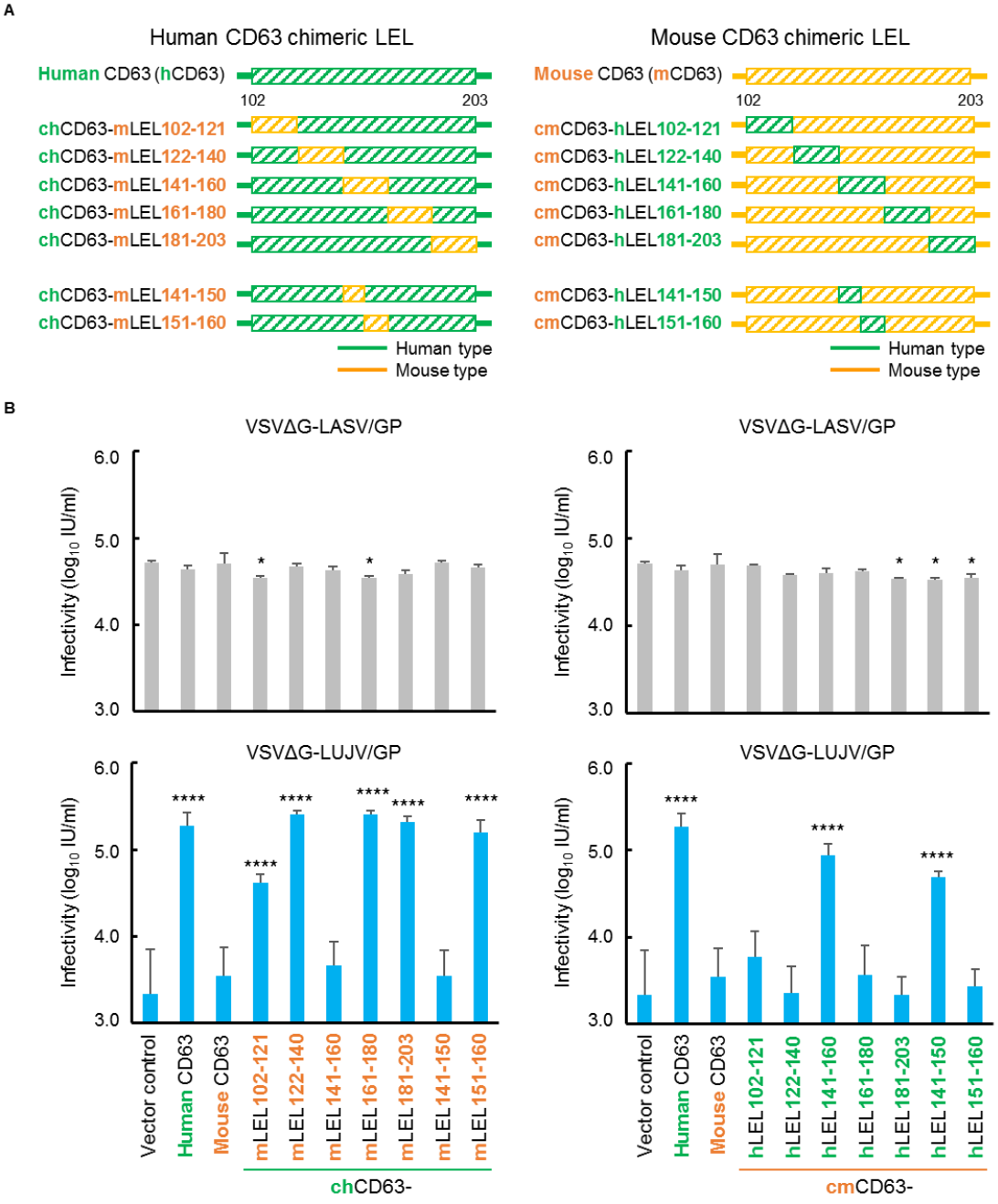

Figure 12. Importance of amino acid positions 141-160 of human CD63 for VSVΔG-LUJV/GP entry. (A) Schematic diagrams of chimeric human and mouse CD63s. The green and yellow colors indicate the regions derived from human and mouse CD63s, respectively. (B) BHK cells expressing wildtype human, mouse, and chimeric CD63s were infected with VSVΔG-LUJV/GP or VSVΔG-LASV/GP. The infectious units (IU) were determined as described in Materials and Methods. Each experiment was conducted three times, and averages and standard deviations are shown. Significant differences compared to the cells transduced with the vector control (Vector control) are shown (*$P < 0.05$, **$P < 0.01$, ***$P < 0.001$, ****$P < 0.0001$).

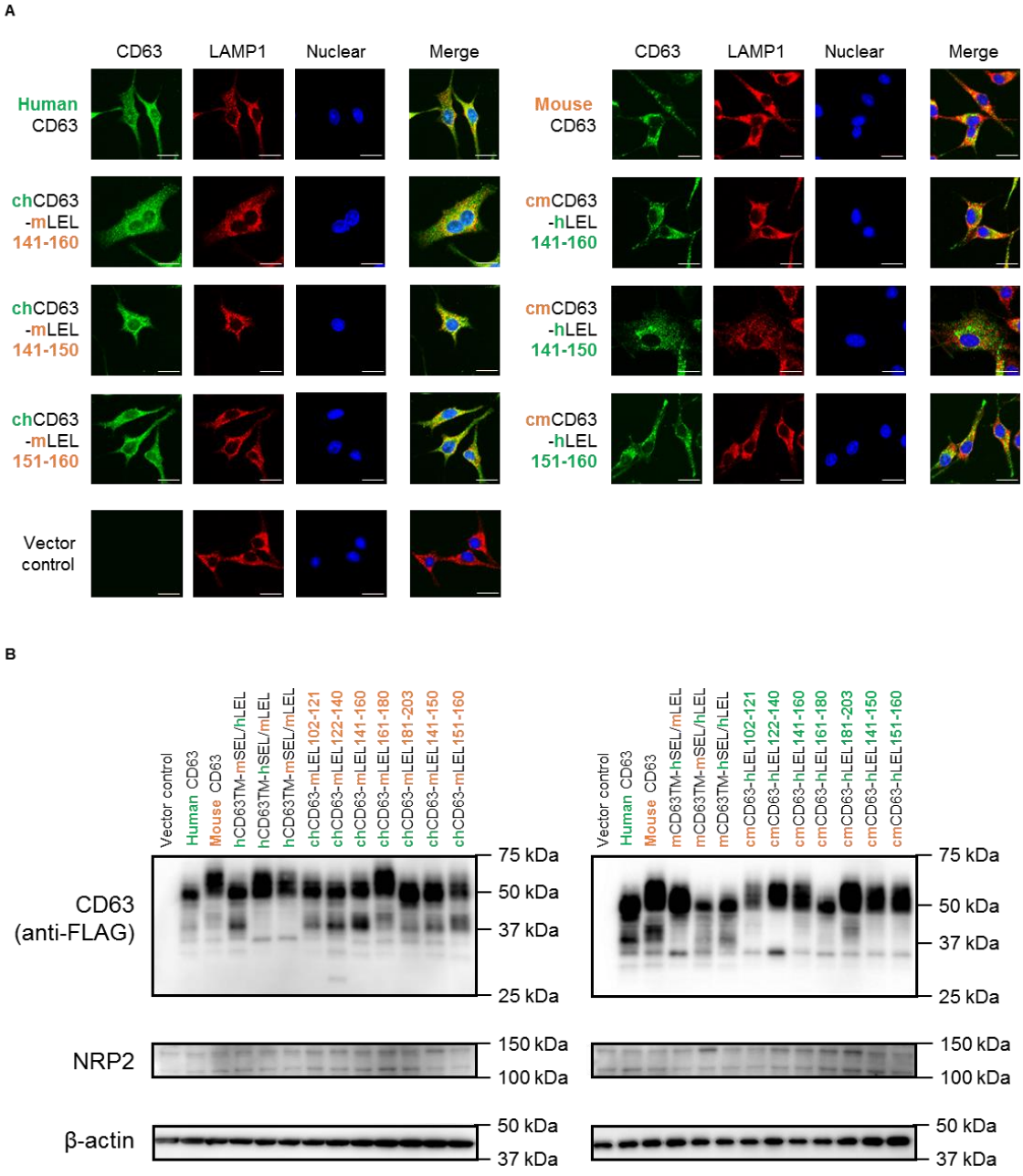

Figure 13. Expression of exogenous human and mouse CD63s and their mutants having the chimeric LEL regions in BHK cells. (A) The intracellular localization of CD63 in BHK cells was analyzed by confocal microscopy as described in Materials and Methods. The scale bars represent 20 μm. (B) Each cell lysate was separated in SDS-PAGE followed by western blotting as described in Materials and Methods.

Importance of the phenylalanine at position 143 in human CD63 for VSVΔG-LUJV/GP infection

In the 141-150 amino acid region, there are five amino acid differences between human and mouse CD63 (Figure 14A). To determine which amino acid residue(s) contributed to the LUJV cellular entry, I generated CD63 mutants containing point mutations at each amino acid position. In these CD63 mutants, the different amino acid residues were swapped between human and mouse CD63s (Figure 14A). Then BHK cells stably expressing these CD63 mutants were produced and their susceptibilities to VSVΔG-LUJV/GP and VSVΔG-LASV/GP were compared (Figure 14B). The protein expression and intracellular localization were confirmed as described above (Figure 15). As with human and mouse wildtype CD63s, the expression of all these CD63 mutants in BHK cells did not significantly affect the efficiency of the VSVΔG- LASV/GP entry (Figure 14, upper panels). In contrast, swapping of the phenylalanine and asparagine residues at position 143 between human and mouse CD63s completely exchanged the susceptibilities of the exogenous CD63-expressing cells to VSVΔG-LUJV/GP (Figure 14, lower panels). These results indicated that the amino acid at position 143 was responsible for the differential susceptibility between the human and mouse cell lines (i.e., HEK293T and NIH3T3) to VSVΔG-LUJV/GP infection.

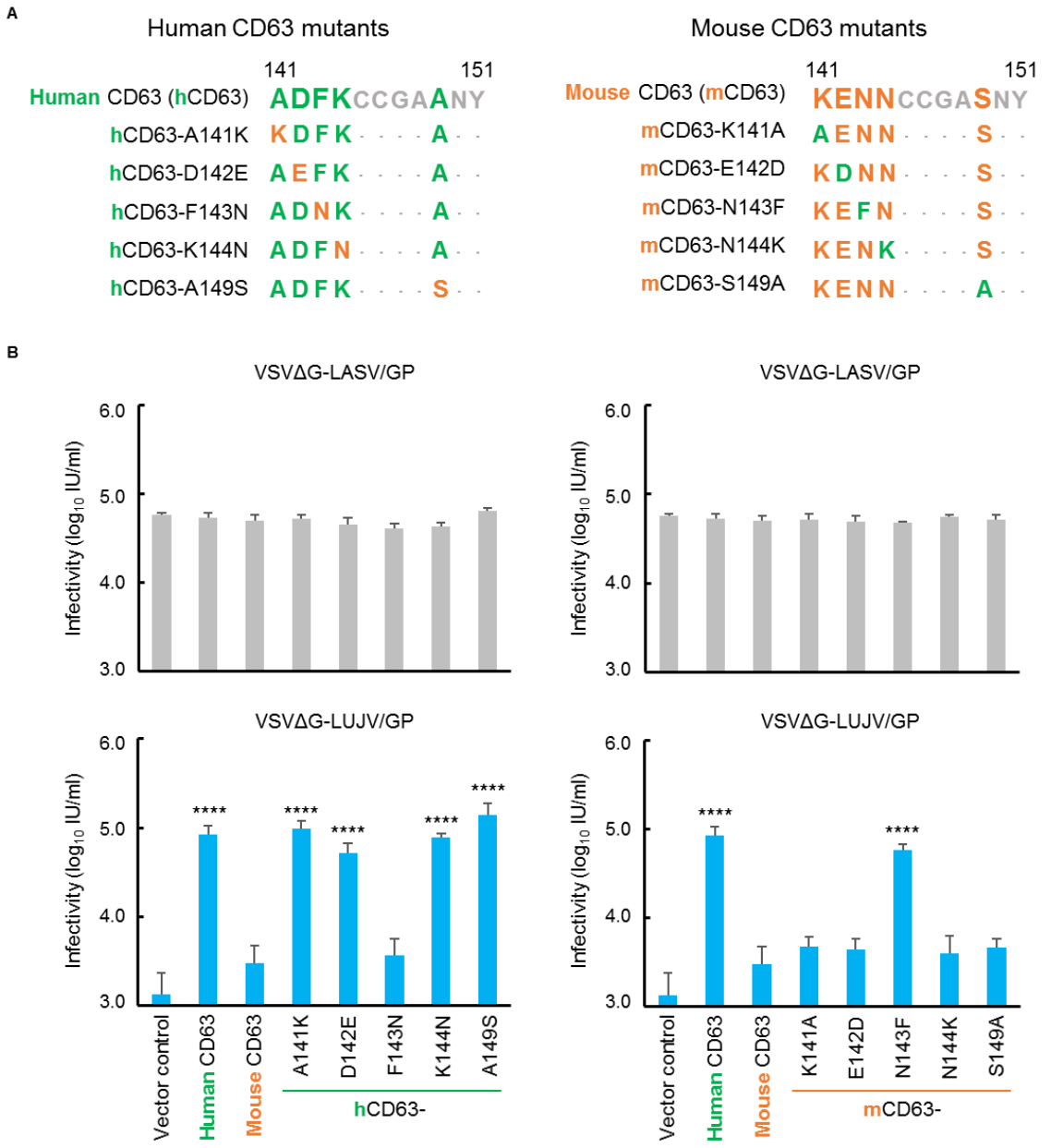

Figure 14. Importance of the amino acid residue at position 143 of human CD63 for VSVΔG-LUJV/GP entry. (A) Amino acid sequences at positions 141-151 of the wildtype human, mouse, and mutant CD63s produced in this study. The green and yellow colors indicate the amino acid residues from human and mouse CD63s, respectively. (B) BHK cells expressing these CD63s were infected with VSVΔG-LUJV/GP or VSVΔG-LASV/GP. The infectious units (IU) were determined as described in Materials and Methods. Each experiment was conducted three times, and averages and standard deviations are shown. Significant differences compared to the cells transduced with the vector control (Vector control) are shown (*$P < 0.05$, **$P < 0.01$, ***$P < 0.001$, ****$P < 0.0001$).

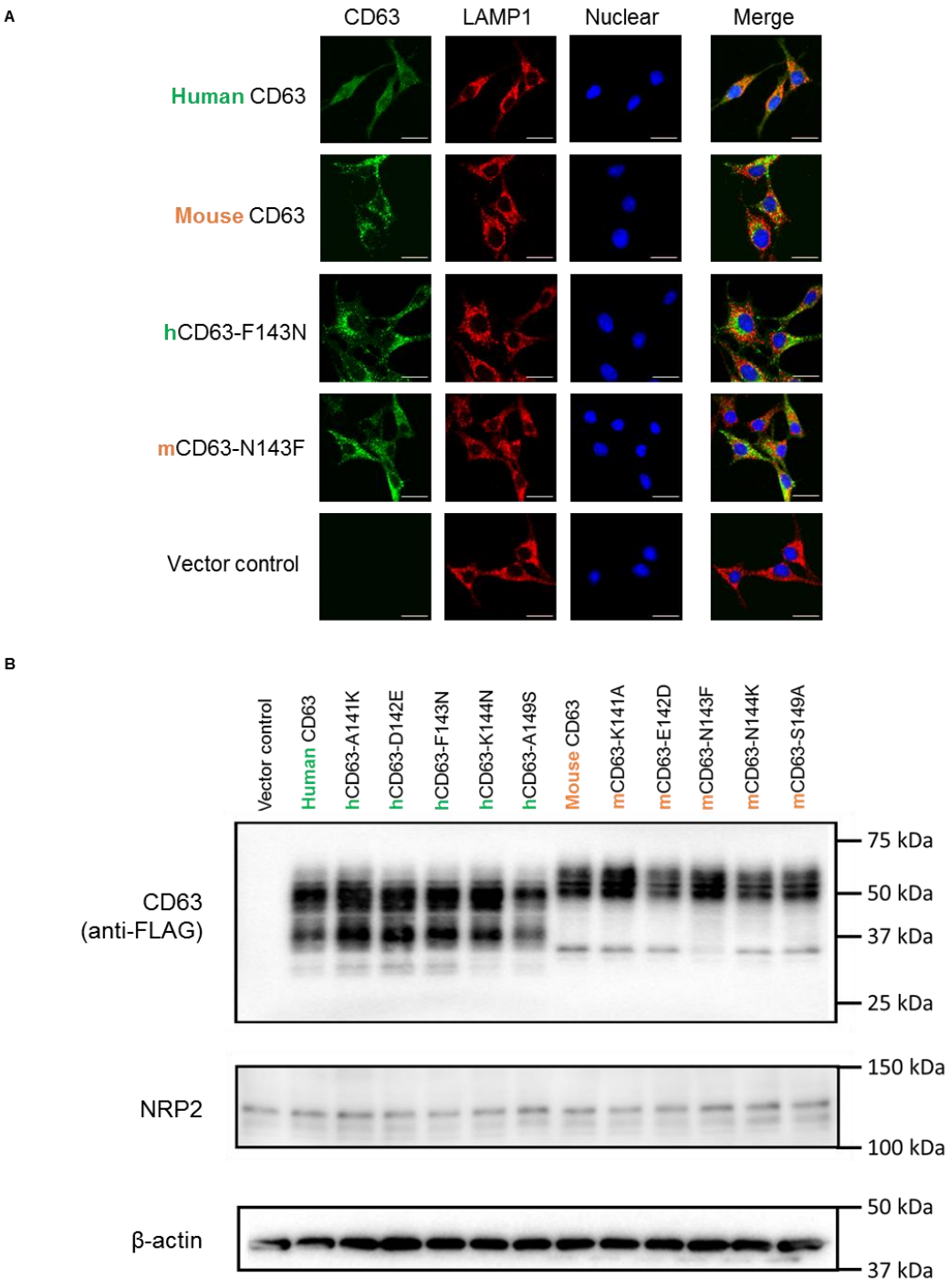

Figure 15. Expression of exogenous human and mouse CD63s and their mutants with single amino acid substitutions in BHK cells. (A) The intracellular localization of CD63 in BHK cells was analyzed by confocal microscopy as described in Materials and Methods. The scale bars represent 20 μm. (B) Each cell lysate was separated in SDS-PAGE followed by western blotting as described in Materials and Methods.

Effects of the amino acid substitution at position 143 of CD63 on LUJV GP-mediated membrane fusion

It has been thought that low pH-activated LUJV GP is released from the attachment receptor NRP2 following conformational change and then interacts with the endosomal fusion receptor CD63 (i.e., receptor switch), leading to membrane fusion. To investigate membrane fusion activity mediated by the interaction between LUJV GP and CD63, I performed a quantitative reporter fusion assay using HEK293 cells expressing LUJV GP and cell-surface-localized exogenous CD63 (i.e., GY234AA mutant) (Figure 16). At neutral pH, appreciable syncytium formation was not detected in any of the CD63-expressing cells. In contrast, significantly increased luciferase activity was observed at low pH in the cells expressing WT human CD63 GY234AA mutant or a mouse CD63 GY234AA mutant having a single mutation (mCD63-N143F), whereas the cells expressing wildtype mouse CD63 or a human CD63 GY234AA mutant with the converse mutation (hCD63-F143N) only showed limited fusion activity, like vector control cells. These data indicated that the differential susceptibility between the human and mouse cell lines was determined by the ability of CD63 to mediate membrane fusion, and that the amino acid residue at position 143 played a major role in the interaction with LUJV GP.

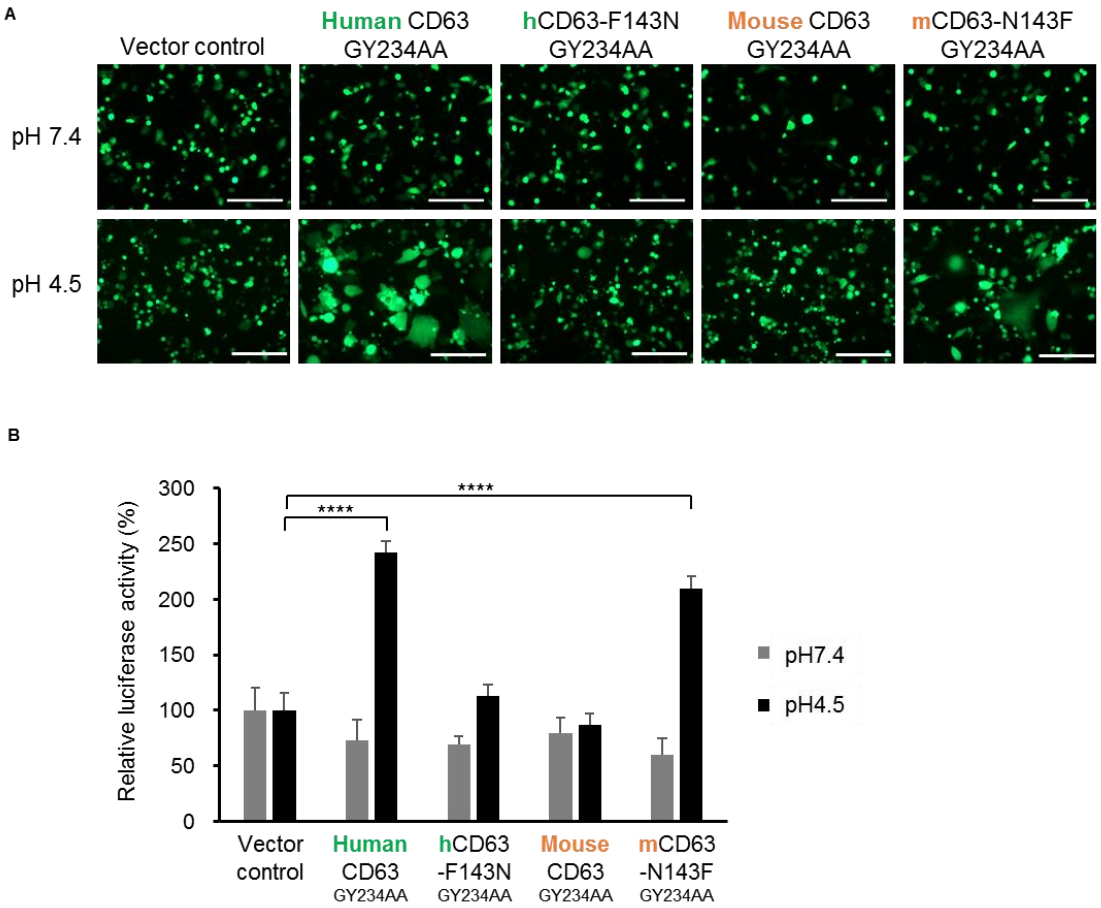

Figure 16. Importance of the amino acid residue at position 143 of human CD63 for LUJV GP-mediated cell fusion. (A) Syncytium formation assays for LUJV GP expressing HEK293 cells after treatment with low and neutral pH buffers (4.5 and 7.4 respectively) were performed as described in Materials and Methods. Syncytium formation was observed by fluorescent microscopy after 24-hour incubation. The scale bars represent 200 μm. (B) Cell fusion activity after exposure at low and neutral pH (4.5 and 7.4, respectively) for 10 min was quantitatively detected as described in Materials and Methods. Each experiment was conducted three times, and averages and standard deviations are shown. Relative luciferase activity was calculated for each pH condition, setting the value of the vector control to 100%. Significant differences compared to the vector control cells (Vector control) are shown (*$P < 0.05$, **$P < 0.01$, ***$P < 0.001$, ****$P < 0.0001$).

Discussion

LUJV caused an outbreak in Zambia and South Africa in 2008 [10]. The nosocomial transmission in this outbreak indicated that LUJV caused human-to-human transmission. Since then, patients with LUJV infection have never been reported and LUJV has never been detected in any animal species [76,77,86]. Although LUJV is classified into the OW arenavirus group because of its discovery in Africa, it is phylogenetically distinct from the other OW arenaviruses, including LASV [10]. In accordance with the structural difference of the GP1 molecule between LUJV and LASV, LUJV utilizes a unique cellular attachment factor, NRP2 [16]. With pH reduction in the endosome, LASV and LUJV GPs switch their binding partners from attachment receptors to the intracellular fusion receptors LAMP1 and CD63, respectively [16,23]. It has been shown that LAMP1 is the key factor for LASV host restriction and that the chicken LAMP1 ortholog lacking the specific N-glycosylation site does not mediate LASV infection [22,23]. Thus, the difference in the receptor usage likely affects the host ranges and natural host preferences of arenaviruses [33]. In the present study, I found that VSVΔG-LASV/GP infected the mouse and hamster cell lines more efficiently than VSVΔG-LUJV/GP. It may be important to note that human and mouse LAMP1 share an N-glycosylation site that is critical for LASV infection [22,23], and this could explain the relatively high susceptibility of the rodent cell lines to VSVΔG-LASV/GP infection. On the other hand, I found that there were considerable amino acid differences between human and mouse CD63s and that the substantially low susceptibility of the mouse cell line to VSVΔG-LUJV/GP was due to the reduced ability of mouse CD63 to mediate membrane fusion. Interestingly, the importance of the endosomal fusion receptor in differential host tropisms of filoviruses has also been reported [27,28,30]. These observations imply a common concept explaining the molecular mechanism underlying viral host ranges controlled by their endosomal fusion receptors.

CD63 is a tetraspanin involved in a variety of cellular processes such as cell activation and cell adhesion [85,87]. It is expressed ubiquitously in late endosomes, lysosomes, and on cell surfaces. For the intracellular localization of CD63, the TM domains are known to be important [85]. Consistent with the fact that the amino acid sequences of the TM region are almost identical in human and mouse CD63s, the localizations of CD63 were similar in them as shown in Figure 11A. Accordingly, my data showed that the exchange of their transmembrane domains did not affect VSVΔG-LUJV/GP infectivity in the CD63-transduced BHK cells, confirming that the TM region was not critical for the difference in susceptibility between the human and mouse cell lines.

My data suggest that LUJV GP interacts with the LEL region of CD63 and that the amino acid residues at positions 141-150 of human CD63, especially the phenylalanine residue at position 143, are essential for GP-mediated membrane fusion and thus for LUJV entry into cells. I attempted to analyze the direct interaction between LUJV GP and human CD63, the human CD63 F143N mutant, mouse CD63, and mouse CD63 N143F mutant by an immunoprecipitation assay but could not detect direct binding of these molecules (data not shown) consistent with a previous study [11]. I assume that the binding affinity between LUJV GP and CD63 might be weak and the presence of detergents during immunoprecipitation assays interfered with the binding of these molecules. However, my fusion assay strongly suggests that the interaction between LUJV GP and CD63 is crucial to mediate membrane fusion.

It should be noted that human CD63 having the 102-121 amino acid region of mouse CD63 (chCD63-mLEL102-121) showed reduced ability to mediate the VSVΔG-LUJV/GP entry, although its impact was lower than the 141-150 region (Figure 12B). In contrast, mouse CD63 having the 102-121 amino acid region of human CD63 (cmCD63-hLEL102-121) did not increase the susceptibility of the transduced BHK cells to VSVΔG-LUJV/GP. This partial negative effect on human CD63 might be due to the difference of N-glycosylation motifs between human and mouse CD63. Mouse CD63, but not human CD63, contains an additional N-glycosylation motif in the 102-121 region (positions 116-118; N-K-S) (Figure 10). It is conceivable that the contact of LUJV GP with the phenylalanine at position 143 on chCD63-mLEL102-121 might be interfered with by this additional glycan derived from the mouse 102-121 sequence.

For the development of antivirals that inhibit viral entry into cells, it is important to clarify the structural bases and molecular mechanisms of the interactions between viral surface proteins and their receptors. For example, the interaction between the E2 glycoprotein of hepatitis C virus (HCV) and CD81, another tetraspanin, has been well investigated [88,89]. The crystal structure of the complex of the HCV E2 glycoprotein and CD81 was resolved and the receptor binding region of the E2 glycoprotein has been identified [90]. The receptor binding regions of the E glycoprotein are targeted by multiple neutralizing antibodies [91]. As antiviral drug candidates that inhibit the entry step of HCV, small chemical compounds mimicking the CD81 LEL partial structure were reported to block the binding of the E glycoprotein to CD81 [92,93]. As is the case with the interaction between CD81 and the HCV E2 glycoprotein, the molecular interface between the CD63 LEL region and LUJV GP may also be a target for neutralizing antibodies and antiviral drugs that block the entry of the virus into host cells.

Since LUJV infection was first reported in 2008, LUJV has not been found anywhere and information on its host range and natural hosts has also been quite limited. Interestingly, the phenylalanine at position 143 (human CD63 numbering) of CD63 orthologs is conserved in many mammalian species (Figure 17). In general, natural hosts of arenaviruses are restricted by geographical and molecular factors, but my data may imply that LUJV has a larger host range than the other arenaviruses. However, some small rodent species such as *Mus musculus* (mouse), *Rattus norvegicus* (rat), and *Mastomys coucha* (Southern multimammate mouse) have different amino acid residues at this position. It has been shown that laboratory mice are resistant to LUJV infection whereas guinea pigs are highly susceptible to the virus and the infection causes fatal disease [35]. Interestingly, CD63 of guinea pigs contains the human-type amino acid residue (phenylalanine) at position 143, which may explain the high susceptibility of this animal species to LUJV infection. On the other hand, my data suggest that hamster CD63 is not fully capable of mediating LUJV entry, although it has a phenylalanine at this amino acid position. To investigate the contribution of the 141-150 amino acid region of hamster CD63, I produced transduced cells expressing chimeric human CD63s having the 141-150 amino acid region from the hamster, Southern multimammate mouse, or rat CD63 and investigated their susceptibilities to VSVΔG-LUJV/GP (data not shown). The cells expressing the chimeric human CD63 having the 141-150 amino acid region of hamster CD63 were found to have enhanced susceptibility to VSVΔG-LUJV/GP. This suggests that other region(s) of CD63 might also be involved in the reduced susceptibility of BHK cells to VSVΔG-LUJV/GP.

In this report, I focused on the distinct susceptibilities of human- and mouse-derived cell lines to VSVΔG-LUJV/GP and identified a molecular factor that is important for the interaction between LUJV GP and CD63 as well as for host tropism of LUJV. Information on the host range and natural hosts of LUJV is a prerequisite for the establishment of epidemiological control strategies, and elucidation of the molecular mechanisms of LUJV entry into cells is critical for the development of effective anti-LUJV drugs. My data provide important information on the possible host range of LUJV and on a potential drug target that inhibits LUJV entry into cells.

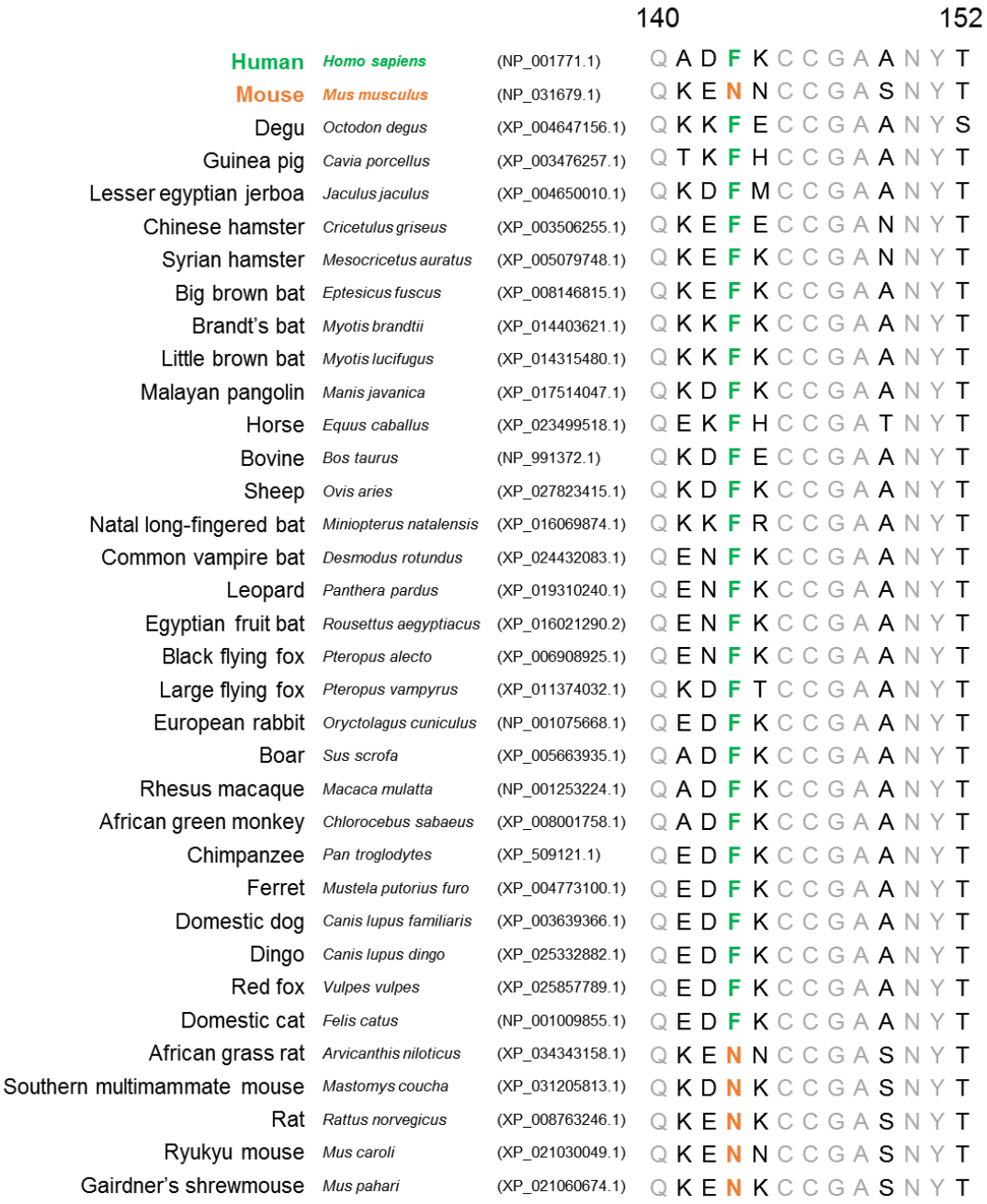

Figure 17. Comparison of amino acid sequences at positions 140-152 of CD63 among mammalian species. Amino acid residues at positions 140-152 (human CD63 numbering) are shown. Gene bank accession numbers are shown in parentheses. Amino acid residues shared among all examined animal species are shown in gray.

Summary

Like other human-pathogenic arenaviruses, LUJV is a causative agent of viral hemorrhagic fever in humans. LUJV infects humans with high mortality rates but the susceptibilities of other animal species and molecular determinants of its host specificity remain unknown. We found that mouse- and hamster-derived cell lines (NIH3T3 and BHK, respectively) were less susceptible to VSVΔG-LUJV/GP than human-derived cell lines (HEK293T and Huh7). To determine the cellular factors involved in the differential susceptibility between the human and mouse cell lines, we focused on the CD63 molecule, which is required for pH-activated GP-mediated membrane fusion during LUJV entry into host cells. The exogenous introduction of human CD63, but not mouse or hamster CD63, into BHK cells significantly increased the susceptibility to VSVΔG-LUJV/GP. Using chimeric human-mouse CD63 proteins, we found that the amino acid residues at positions 141-150 in the LEL region of CD63 were important for the cellular entry of VSVΔG-LUJV/GP. By site-directed mutagenesis, we further determined that a phenylalanine at position 143 in human CD63 was the key residue for efficient membrane fusion and VSVΔG-LUJV/GP infection. Our data suggest that the interaction of LUJV GP with the LEL region of CD63 is essential for cell susceptibility to LUJV, thus providing new insights into the molecular mechanisms underlying the cellular entry of LUJV and host range restriction of this virus.

Conclusion

For filoviruses and arenaviruses, the interaction of viral surface glycoproteins (GPs) and cell surface receptors is the initial step of entry, followed by incorporation of virus particles into endosomes. Filoviruses represented by EBOV and MARV, and some members of arenavirus such as LASV and LUJV, require intercellular receptors for fusion between viral envelope and endosomal membrane. In general, the GP-receptor engagement is an important determinant for the tissue tropism, pathogenicity, and host specificities of the viruses. Thus, it is important to investigate the function and property of GPs for better understanding of viral pathogenesis as well as for the establishment of countermeasures to control infectious diseases caused by these viruses.

In chapter I, it was demonstrated that rVSV/EBOV and rVSV/MARV caused lethal infection in Syrian hamsters and the tissue tropisms of these viruses were partially similar to those of EBOV and MARV infection in humans. Elevated levels of liver enzymes and thrombocytopenia, both of which are typically found in EBOV infection of humans, were also found in rVSV/EBOV-infected hamsters. These results suggest that their tissue tropisms and some of the physiological events depend on the function of EBOV and MARV GPs. Using this model, I further confirmed therapeutic effects of passive immunization with neutralizing anti-EBOV GP monoclonal antibody. This surrogate animal model of filovirus infection is a useful tool for screening of drugs targeting the filovirus GP functions under BSL-2 conditions and is expected to accelerate drug and vaccine development.

In chapter II, I revealed the mechanisms underlying the differential susceptibilities between human and rodent cell lines to LUJV infection, focusing on the function of LUJV GP. I infected several cell lines with VSVΔG-LUJV/GP and found that rodent-derived cell lines were less susceptible than human-derived cell lines. Then, the differential susceptibilities were found to be determined by the structural difference of CD63, the intercellular receptor of LUJV. I further identified an important amino acid residue on human CD63 for efficient LUJV infection and found that this amino acid was shared among many animal species. These results suggest that the interaction between LUJV GP and CD63 is one of the important factors to determine the host range of JUJV and that LUJV potentially has larger host range than other arenaviruses.

In the present study, I focused on the cell tropism of hemorrhagic fever viruses and mechanisms of entry into cells. The surrogate animal models of EBOV and MARV infection established in this study is expected to be widely used for evaluation of the filovirus pathogenicity depending on the GP tropism and screening of antiviral drugs targeting GPs. The findings on the CD63-regulated susceptibilities of the cell lines to

LUJV infection provide important information for the development of anti-LUJV drugs as well as identification of natural hosts of LUJV.

Acknowledgments

I express my deepest gratitude to my supervisor, Prof. Ayato Takada (Division of Global Epidemiology, Research Center for Zoonosis Control [CZC], Hokkaido University [HU]). He gave me accurate advice and encouragement during my PhD course. He also gave me many opportunities abroad for field work.

I sincerely appreciate invaluable advice and suggestion from Prof. Hirofumi Sawa (Division of Molecular pathology, CZC, HU), Prof. Takashi Kimura (Laboratory of Comparative Pathology, Graduate School of Veterinary Medicine, HU), and Senior Lecturer. Keita Matsuno (Unit of Risk Analysis and Management, CZC, HU) for my research work.

I'm deeply grateful to Associate Prof. Manabu Igarashi, Assistant Prof. Masahiro Kajihara (Division of Global Epidemiology, CZC, HU). They gave me technical and intellectual supports.

I am indebted to Specially Appointed Prof. Hiroshi Kida (CZC, HU), Associate Prof. Osamu Ichii (Laboratory of Anatomy, Graduate School of Veterinary Medicine, HU), and Assistant Prof. Hirohito Ogawa (Graduate School of Medicine, Dentistry and Pharmaceutical Sciences, Okayama University) for their technical advices and supports.

I would like to thank to Dr. Junki Maruyama, Dr. Wakako Furuyama, Dr. Tatsunari Kondoh, Dr. Masahiro Sato, Dr. Yoshihiro Takadate, and Ms. Hiroko Miyamoto (Division of Global Epidemiology, CZC, HU) for their advices and suggestions.

I also thank to Mr. Mao Isono, Mr. Kosuke Okuya, Mr. Boniface Lombe Pongombo, Ms. Nodoka Kasajima, Ms. Yurie Kida, Mr. Takanari Hattori, Mr. Yuji Takahashi, Ms. Akina Mori-Kajihara, and Mr. Suguru Taga (Division of Global Epidemiology, CZC, HU) for their daily assistance.

I also express my deep gratitude to my family for their understanding and financial supports for a long period.

Abstract in Japanese

出血熱を引き起こすウイルスは主に 7 つのウイルス科（フィロウイルス科、アレナウイルス科、フラビウイルス科、ナイロウイルス科、ハンタウイルス科、フェニュイウイルス科、パラミクソウイルス科）に属する。これらのウイルスはエンベロープを有する、マイナス鎖 RNA ウイルスである。フィロウイルス科に属する Ebola virus（EBOV）および Marburg virus（MARV）や、アレナウイルス科に属する Lassa virus（LASV）および Lujo virus（LUJV）などによるウイルス性出血熱の致死率は高く、これらのウイルスは Biosafety level (BSL)-4 施設で扱わなければならない病原体として分類されている。EBOV、MARV、LASV および LUJV の細胞侵入過程において、表面糖蛋白質 GP が宿主細胞に発現しているレセプターに結合することが必須である。GP はウイルスの標的細胞決定に重要であるとともに、中和抗体などの治療薬のターゲットである。また、GP とレセプターの相互作用は宿主特異性を規定する因子でもある。本論文では EBOV、MARV、LASV および LUJV の GP により規定される細胞指向性と細胞侵入メカニズムに関する研究を行った。

EBOV と MARV に代表されるフィロウイルスはヒトを含む霊長類に高い致死率の出血熱を引き起こす。これらのフィロウイルス感染症に対するワクチンや治療法は限られており、その原因の一つとして、実験を BSL-4 施設で行わなければならない制限が挙げられる。第一章では BSL-2 あるいは BSL-3 施設で抗フィロウイルス薬のスクリーニング実施が可能な代替動物実験モデルの確立を試みた。まず、EBOV と MARV の表面糖蛋白質（GP）に注目し、水胞性口炎ウイルス（VSV）の G 蛋白質遺伝子を EBOV および MARV の GP 遺伝子に置換した組換えウイルス（rVSV/EBOV および rVSV/MARV）を作出した。動物種ごとの感受性を比較するために rVSV/EBOV をマウス、ラットおよびシリアンハムスターに感染させたところ、シリアンハムスターでのみ顕著な体重減少が認められ、rVSV/EBOV 感染ハムスターは感染後 4 日以内で死亡した。rVSV/MARV も同様にハムスターに対して致死的感染を引き起こした。rVSV/EBOV および rVSV/MARV 感染ハムスターの全身の臓器でウイルスの増殖が認められた。特に、肝臓、脾臓、腎臓および肺でのウイルス感染価が高かった。病理学的解析から、VSV が肝細胞、単球、リンパ球および神経細胞といった広範囲な細胞に感染していたのに比較して、rVSV/EBOV と rVSV/MARV では肝細胞、マクロファージおよび単球系細胞といった実際の EBOV および MARV が標的とする細胞に感染する傾向がある事が分かった。また、rVSV/EBOV 感染ハムスターでは白血球数の減少および AST と ALP の上昇がみられ、ヒトの EBOV 感染でみられる臨床所見との類似点が認められた。以上の結果から、rVSV/EBOV と rVSV/MARV の組織特異性や病原性には GP が強く関与していることが示唆された。次に、rVSV/EBOV 感染前後に抗 EBOV 中和抗体を投与したところ、体重減少の消失と致死率の低下といった治療効果が認められた。これらの結果は、このフィロウイルス感染代替動物モデルは GP に作用する中和抗体や化合物などの抗フィロウイ

ルス薬の *in vivo* スクリーニングに有用である事を示している。

第二章では、哺乳類アレナウイルス属に属するルジョウイルス（LUJV）に対する細胞感受性を規定する宿主因子に関する研究を行った。LUJV は 2008 年にザンビアおよび南アフリカで小規模のウイルス性出血熱の流行を引き起こしたウイルスであり、感染者 5 人中 4 人が死亡した。しかし、2008 年以降、LUJV 感染の報告はなく、加えてげっ歯類を対象とした疫学調査においても LUJV は検出されておらず、LUJV の生態、宿主域および自然宿主に関する知見は殆どない。本研究では、まず LUJV の表面糖蛋白質 GP を纏ったシュードタイプウイルス（VSVΔG-LUJV/GP）に対する細胞株の感受性を比較したところ、ヒト由来の細胞株（Huh7、HEK293T）は高感受性であったのに対し、マウス由来細胞株（NIH3T3）とハムスター由来細胞株（BHK）は低感受性であることが分かった。そこで、この感受性の違いに関与する宿主因子の解析を行った。LUJV の細胞内侵入に関わる宿主因子として Neuropilin 2（NRP2）と CD63 が報告されている。CD63 は LUJV の細胞内侵入過程における膜融合レセプターとして報告されている。NRP2 のアミノ酸配列を比較したところ、LUJV の GP との相互作用に重要な CUB1 領域における配列の違いは、ヒト、マウスおよびハムスターの間でほとんど認められなかった事から CD63 に着目した。VSVΔG-LUJV/GP に殆ど感受性を示さなかった BHK 細胞に、ヒト、マウスおよびハムスターCD63 を発現させたところ、ヒト CD63 を発現させた場合のみ VSVΔG-LUJV/GP に対する感受性が有意に上昇した。この結果は CD63 がヒトとげっ歯類細胞株間における LUJV に対する感受性を規定していることを示している。次に、ヒト CD63 において LUJV 感染に重要である領域を探索した。ヒトとマウス CD63 のキメラ CD63 を BHK 細胞に発現させ、VSVΔG-LUJV/GP の感染性の変化を解析した結果、ヒト CD63 の Large extracellular loop（LEL）領域が LUJV 感染に重要である事が分かった。さらに、LEL 領域の 141 番目から 150 番目のアミノ酸、特に 143 番目のフェニルアラニンが LUJV 感染に重要であることが示唆された。また、このアミノ酸は LUJV の GP による膜融合に重要であることが分かった。CD63 の 143 番目のフェニルアラニンはマウスやラットを含む一部のげっ歯類を除いた哺乳類で広く保存されていたことから、LUJV は広い宿主域をもつ可能性が示唆された。

出血熱ウイルスの表面糖蛋白質 GP は細胞侵入過程、組織特異性、宿主域に関与する。このため出血熱ウイルスによる病原性発現を理解し、対策を構築するには機能的 GP の理解および応用が必須である。本研究で構築したフィロウイルス感染代替動物モデルは GP による組織特異性を応用したものであり、GP による病原性発現の評価や GP を狙った抗ウイルス薬の評価に広く利用されることが期待される。また LUJV GP とレセプターの相互作用は LUJV 感受性の決定に重要であることから、特に CD63 が細胞株の感受性を規定することを示した。感染性ウイルスを用いた詳細な解析が期待されるが、本研究で得られた知見は抗 LUJV 薬の開発や宿主域の推定・特定において重要な情報である。

References

1. CDC Virus Families | Viral Hemorrhagic Fevers (VHFs) | CDC Available online: https://www.cdc.gov/vhf/virus-families/index.html (accessed on Dec 9, 2020).
2. Smith, D.R.; Holbrook, M.R.; Gowen, B.B. Animal models of viral hemorrhagic fever. *Antiviral Res.* **2014**, *112*, 59–79.
3. Bugert, J.J.; Hucke, F.; Zanetta, P.; Bassetto, M.; Brancale, A. Antivirals in medical biodefense. *Virus Genes* **2020**, *56*, 150–167.
4. European Medicines Agency Ebola - European Medicines Agency Available online: https://www.ema.europa.eu/en/human-regulatory/overview/public-health-threats/ebola (accessed on Apr 11, 2020).
5. FDA First FDA-approved vaccine for the prevention of Ebola virus disease, marking a critical milestone in public health preparedness and response Available online: https://www.fda.gov/news-events/press-announcements/first-fda-approved-vaccine-prevention-ebola-virus-disease-marking-critical-milestone-public-health (accessed on Apr 11, 2020).
6. Furuyama, W.; Marzi, A. Ebola Virus: Pathogenesis and Countermeasure Development. *Annu. Rev. Virol.* **2019**, *6*, 435–458.
7. Amarasinghe, G.K.; Aréchiga Ceballos, N.G.; Banyard, A.C.; Basler, C.F.; Bavari, S.; Bennett, A.J.; Blasdell, K.R.; Briese, T.; Bukreyev, A.; Caì, Y.; et al. Taxonomy of the order Mononegavirales: update 2018. *Arch. Virol.* **2018**, *163*, 2283–2294.
8. Martines, R.B.; Ng, D.L.; Greer, P.W.; Rollin, P.E.; Zaki, S.R. Tissue and cellular tropism, pathology and pathogenesis of Ebola and Marburg viruses. *J. Pathol.* **2015**, *235*, 153–174.
9. Moraz, M.L.; Kunz, S. Pathogenesis of arenavirus hemorrhagic fevers. *Expert Rev. Anti. Infect. Ther.* **2011**, *9*, 49–59.
10. Briese, T.; Paweska, J.T.; McMullan, L.K.; Hutchison, S.K.; Street, C.; Palacios, G.; Khristova, M.L.; Weyer, J.; Swanepoel, R.; Egholm, M.; et al. Genetic detection and characterization of Lujo virus, a new hemorrhagic fever-associated arenavirus from southern Africa. *PLoS Pathog.* **2009**, *5*, e1000455.
11. Sewlall, N.H.; Richards, G.; Duse, A.; Swanepoel, R.; Paweska, J.; Blumberg, L.; Dinh, T.H.; Bausch, D. Clinical features and patient management of Lujo hemorrhagic fever. *PLoS Negl. Trop. Dis.* **2014**, *8*, e3233.
12. Martin, B.; Hoenen, T.; Canard, B.; Decroly, E. Filovirus proteins for antiviral drug discovery: A structure/function analysis of surface glycoproteins and virus entry. *Antiviral Res.* **2016**, *135*, 1–14.

13. Hallam, S.J.; Koma, T.; Maruyama, J.; Paessler, S. Review of mammarenavirus biology and replication. *Front. Microbiol.* **2018**, *9*, 1751.
14. Takada, A. Filovirus tropism: Cellular molecules for viral entry. *Front. Microbiol.* **2012**, *3*, 1–9.
15. Hofmann-Winkler, H.; Kaup, F.; Pöhlmann, S. Host cell factors in filovirus entry: Novel players, new insights. *Viruses* **2012**, *4*, 3336–3362.
16. Raaben, M.; Jae, L.T.; Herbert, A.S.; Kuehne, A.I.; Stubbs, S.H.; Chou, Y. ying; Blomen, V.A.; Kirchhausen, T.; Dye, J.M.; Brummelkamp, T.R.; et al. NRP2 and CD63 are host factors for Lujo virus cell entry. *Cell Host Microbe* **2017**, *22*, 688-696.e5.
17. Cohen-Dvashi, H.; Kilimnik, I.; Diskin, R. Structural basis for receptor recognition by Lujo virus. *Nat. Microbiol.* **2018**, *3*, 1153–1160.
18. Rojek, J.M.; Kunz, S. Cell entry by human pathogenic arenaviruses. *Cell. Microbiol.* **2008**, *10*, 828–835.
19. Kunz, S. Receptor binding and cell entry of Old World arenaviruses reveal novel aspects of virus-host interaction. *Virology* **2009**, *387*, 245–249.
20. Carette, J.E.; Raaben, M.; Wong, A.C.; Herbert, A.S.; Obernosterer, G.; Mulherkar, N.; Kuehne, A.I.; Kranzusch, P.J.; Griffin, A.M.; Ruthel, G.; et al. Ebola virus entry requires the cholesterol transporter Niemann-Pick C1. *Nature* **2011**, *477*, 340–343.
21. Côté, M.; Misasi, J.; Ren, T.; Bruchez, A.; Lee, K.; Filone, C.M.; Hensley, L.; Li, Q.; Ory, D.; Chandran, K.; et al. Small molecule inhibitors reveal Niemann-Pick C1 is essential for Ebola virus infection. *Nature* **2011**, *477*, 344–348.
22. Jae, L.T.; Brummelkamp, T.R. Emerging intracellular receptors for hemorrhagic fever viruses. *Trends Microbiol.* **2015**, *23*, 392–400.
23. Jae, L.T.; Raaben, M.; Herbert, A.S.; Kuehne, A.I.; Wirchnianski, A.S.; Soh, T.K.; Stubbs, S.H.; Janssen, H.; Damme, M.; Saftig, P.; et al. Lassa virus entry requires a trigger-induced receptor switch. *Science* **2014**, *344*, 1506–1510.
24. Saphire, E.O.; Schendel, S.L.; Gunn, B.M.; Milligan, J.C.; Alter, G. Antibody-mediated protection against Ebola virus. *Nat. Immunol.* **2018**, *19*, 1169–1178.
25. Basu, A.; Li, B.; Mills, D.M.; Panchal, R.G.; Cardinale, S.C.; Butler, M.M.; Peet, N.P.; Majgier-Baranowska, H.; Williams, J.D.; Patel, I.; et al. Identification of a small-molecule entry inhibitor for filoviruses. *J. Virol.* **2011**, *85*, 3106–3119.
26. Isono, M.; Furuyama, W.; Kuroda, M.; Kondoh, T.; Igarashi, M.; Kajihara, M.; Yoshida, R.; Manzoor, R.; Okuya, K.; Miyamoto, H.; et al. A biaryl sulfonamide derivative as a novel inhibitor of filovirus infection. *Antiviral Res.* **2020**, *183*,

104932.
27. Takadate, Y.; Manzoor, R.; Saito, T.; Kida, Y.; Maruyama, J.; Kondoh, T.; Miyamoto, H.; Ogawa, H.; Kajihara, M.; Igarashi, M.; et al. Receptor-mediated host cell preference of a bat-derived filovirus, Lloviu virus. *Microorganisms* **2020**, *8*, 1–12.
28. Ng, M.; Ndungo, E.; Kaczmarek, M.E.; Herbert, A.S.; Binger, T.; Kuehne, A.I.; Jangra, R.K.; Hawkins, J.A.; Gifford, R.J.; Biswas, R.; et al. Filovirus receptor NPC1 contributes to species-specific patterns of ebolavirus susceptibility in bats. *Elife* **2015**, *4*, e11785.
29. Ndungo, E.; Herbert, A.S.; Raaben, M.; Obernosterer, G.; Biswas, R.; Miller, E.H.; Wirchnianski, A.S.; Carette, J.E.; Brummelkamp, T.R.; Whelan, S.P.; et al. A single residue in ebola virus receptor NPC1 influences cellular host range in reptiles. *mSphere* **2016**, *1*, e00007-16.
30. Takadate, Y.; Kondoh, T.; Igarashi, M.; Maruyama, J.; Manzoor, R.; Ogawa, H.; Kajihara, M.; Furuyama, W.; Sato, M.; Miyamoto, H.; et al. Niemann-Pick C1 heterogeneity of bat cells controls filovirus tropism. *Cell Rep.* **2020**, *30*, 308-319.e5.
31. Olayemi, A.; Obadare, A.; Oyeyiola, A.; Igbokwe, J.; Fasogbon, A.; Igbahenah, F.; Ortsega, D.; Asogun, D.; Umeh, P.; Vakkai, I.; et al. Arenavirus diversity and phylogeography of mastomys natalensis Rodents, Nigeria. *Emerg. Infect. Dis.* **2016**, *22*, 694–697.
32. Zapata, J.C.; Salvato, M.S. Arenavirus variations due to host-specific adaptation. *Viruses* **2013**, *5*, 241–278.
33. Charrel, R.N.; Lemasson, J.J.; Garbutt, M.; Khelifa, R.; De Micco, P.; Feldmann, H.; De Lamballerie, X. New insights into the evolutionary relationships between arenaviruses provided by comparative analysis of small and large segment sequences. *Virology* **2003**, *317*, 191–196.
34. Rasmussen, A.L.; Tchitchek, N.; Safronetz, D.; Carter, V.S.; Williams, C.M.; Haddock, E.; Korth, M.J.; Feldmann, H.; Katze, M.G. Delayed inflammatory and cell death responses are associated with reduced pathogenicity in Lujo virus-infected cynomolgus macaques. *J. Virol.* **2015**, *89*, 2543–2552.
35. Bird, B.H.; Dodd, K.A.; Erickson, B.R.; Albariño, C.G.; Chakrabarti, A.K.; McMullan, L.K.; Bergeron, E.; Ströeher, U.; Cannon, D.; Martin, B.; et al. Severe hemorrhagic fever in strain 13/N guinea pigs infected with Lujo virus. *PLoS Negl. Trop. Dis.* **2012**, *6*, e1801.
36. Tani, H.; Iha, K.; Shimojima, M.; Fukushi, S.; Taniguchi, S.; Yoshikawa, T.;

Kawaoka, Y.; Nakasone, N.; Ninomiya, H.; Saijo, M.; et al. Analysis of Lujo virus cell entry using pseudotype vesicular stomatitis virus. *J. Virol.* **2014**, *88*, 7317–7330.

37. Malvy, D.; McElroy, A.K.; de Clerck, H.; Günther, S.; van Griensven, J. Ebola virus disease. *Lancet* **2019**, *393*, 936–948.
38. Martini, G.A. Marburg virus disease. *Postgrad. Med. J.* **1973**, *49*, 542–546.
39. Bente, D.; Gren, J.; Strong, J.E.; Feldmann, H. Disease modeling for Ebola and Marburg viruses. *Dis. Model. Mech.* **2009**, *2*, 12–17.
40. Bradfute, S.B.; Warfield, K.L.; Bray, M. Mouse models for filovirus infections. *Viruses* **2012**, *4*, 1477–1508.
41. Wahl-Jensen, V.; Bollinger, L.; Safronetz, D.; De Kok-Mercado, F.; Scott, D.P.; Ebihara, H. Use of the syrian hamster as a new model of ebola virus disease and other viral hemorrhagic fevers. *Viruses* **2012**, *4*, 3754–3784.
42. Siragam, V.; Wong, G.; Qiu, X.G. Animal models for filovirus infections. *Zool. Res.* **2018**, *39*, 15–24.
43. Nakayama, E.; Saijo, M. Animal models for Ebola and Marburg virus infections. *Front. Microbiol.* **2013**, *4*, 1–20.
44. Marzi, A.; Robertson, S.J.; Haddock, E.; Feldmann, F.; Hanley, P.W.; Scott, D.P.; Strong, J.E.; Kobinger, G.; Best, S.M.; Feldmann, H. VSV-EBOV rapidly protects macaques against infection with the 2014/15 Ebola virus outbreak strain. *Science* **2015**, *349*, 739–742.
45. Marzi, A.; Hanley, P.W.; Haddock, E.; Martellaro, C.; Kobinger, G.; Feldmann, H. Efficacy of vesicular stomatitis virus-ebola virus postexposure treatment in rhesus macaques infected with ebola virus makona. *J. Infect. Dis.* **2016**, *214*, S360–S366.
46. Marzi, A.; Reynolds, P.; Mercado-Hernandez, R.; Callison, J.; Feldmann, F.; Rosenke, R.; Thomas, T.; Scott, D.P.; Hanley, P.W.; Haddock, E.; et al. Single low-dose VSV-EBOV vaccination protects cynomolgus macaques from lethal Ebola challenge. *EBioMedicine* **2019**, *49*, 223–231.
47. Bixler, S.L.; Bocan, T.M.; Wells, J.; Wetzel, K.S.; Van Tongeren, S.A.; Dong, L.; Garza, N.L.; Donnelly, G.; Cazares, L.H.; Nuss, J.; et al. Efficacy of favipiravir (T-705) in nonhuman primates infected with Ebola virus or Marburg virus. *Antiviral Res.* **2018**, *151*, 97–104.
48. Guedj, J.; Piorkowski, G.; Jacquot, F.; Madelain, V.; Nguyen, T.H.T.; Rodallec, A.; Gunther, S.; Carbonnelle, C.; Mentré, F.; Raoul, H.; et al. Antiviral efficacy of favipiravir against Ebola virus: A translational study in cynomolgus macaques.

PLoS Med. **2018**, *15*, e1002535.

49. Connolly, B.M.; Steele, K.E.; Davis, K.J.; Geisbert, T.W.; Kell, W.M.; Jaax, N.K.; Jahrling, P.B. Pathogenesis of experimental Ebola virus infection in guinea pigs. *J. Infect. Dis.* **1999**, *179*, S203-17.
50. Marzi, A.; Kercher, L.; Marceau, J.; York, A.; Callsion, J.; Gardner, D.J.; Geisbert, T.W.; Feldmann, H. Stat1-deficient mice are not an appropriate model for efficacy testing of recombinant vesicular stomatitis virus-based filovirus vaccines. *J. Infect. Dis.* **2015**, *212*, S404–S409.
51. Qiu, X.; Wong, G.; Audet, J.; Cutts, T.; Niu, Y.; Booth, S.; Kobinger, G.P. Establishment and characterization of a lethal mouse model for the Angola strain of Marburg virus. *J. Virol.* **2014**, *88*, 12703–12714.
52. Comer, J.E.; Escaffre, O.; Neef, N.; Brasel, T.; Juelich, T.L.; Smith, J.K.; Smith, J.; Kalveram, B.; Perez, D.D.; Massey, S.; et al. Filovirus virulence in interferon α/β and γ double knockout mice, and treatment with favipiravir. *Viruses* **2019**, *11*, 137.
53. Ebihara, H.; Takada, A.; Kobasa, D.; Jones, S.; Neumann, G.; Theriault, S.; Bray, M.; Feldmann, H.; Kawaoka, Y. Molecular determinants of Ebola virus virulence in mice. *PLoS Pathog.* **2006**, *2*, 0705–0711.
54. Bray, M.; Davis, K.; Geisbert, T.; Schmaljohn, C.; Huggins, J. A mouse model for evaluation of prophylaxis and therapy of ebola hemorrhagic fever. *J. Infect. Dis.* **1998**, *178*, 651–661.
55. Wong, G.; Cao, W.G.; He, S.H.; Zhang, Z.R.; Zhu, W.J.; Moffat, E.; Ebihara, H.; Embury-Hyatt, C.; Qiu, X.G. Development and characterization of a guinea pig model for Marburg virus. *Zool. Res.* **2018**, *39*, 32–41.
56. Marzi, A.; Banadyga, L.; Haddock, E.; Thomas, T.; Shen, K.; Horne, E.J.; Scott, D.P.; Feldmann, H.; Ebihara, H. A hamster model for Marburg virus infection accurately recapitulates Marburg hemorrhagic fever. *Sci. Rep.* **2016**, *6*, 39214.
57. Bray, M. The role of the type I interferon response in the resistance of mice of filovirus infection. *J. Gen. Virol.* **2001**, *82*, 1365–1373.
58. Ebihara, H.; Zivcec, M.; Gardner, D.; Falzarano, D.; Lacasse, R.; Rosenke, R.; Long, D.; Haddock, E.; Fischer, E.; Kawaoka, Y.; et al. A syrian golden hamster model recapitulating ebola hemorrhagic fever. *J. Infect. Dis.* **2013**, *207*, 306–318.
59. Takada, A.; Feldmann, H.; Stroeher, U.; Bray, M.; Watanabe, S.; Ito, H.; McGregor, M.; Kawaoka, Y. Identification of protective epitopes on Ebola virus glycoprotein at the single amino acid level by using recombinant vesicular stomatitis viruses. *J. Virol.* **2003**, *77*, 1069–1074.

60. Garbutt, M.; Liebscher, R.; Wahl-Jensen, V.; Jones, S.; Möller, P.; Wagner, R.; Volchkov, V.; Klenk, H.-D.; Feldmann, H.; Ströher, U. Properties of replication-competent vesicular stomatitis virus vectors expressing glycoproteins of filoviruses and arenaviruses. *J. Virol.* **2004**, *78*, 5458–5465.
61. Marzi, A.; Feldmann, H.; Geisbert, T.W.; Falzarano, D. Vesicular stomatitis virus-based vaccines for prophylaxis and treatment of filovirus infections. *J. Bioterror. Biodef.* **2011**, *S1(4)*, 2157-2526-S1-004.
62. Tsuda, Y.; Safronetz, D.; Brown, K.; Lacasse, R.; Marzi, A.; Ebihara, H.; Feldmann, H. Protective efficacy of a bivalent recombinant vesicular stomatitis virus vaccine in the syrian hamster model of lethal Ebola virus infection. *J. Infect. Dis.* **2011**, *204*, S1090-1097.
63. Suder, E.; Furuyama, W.; Feldmann, H.; Marzi, A.; de Wit, E. The vesicular stomatitis virus-based Ebola virus vaccine: From concept to clinical trials. *Hum. Vaccines Immunother.* **2018**, *14*, 2107–2113.
64. McWilliams, I.L.; Kielczewski, J.L.; Ireland, D.D.C.; Sykes, J.S.; Lewkowicz, A.P.; Konduru, K.; Xu, B.C.; Chan, C.C.; Caspi, R.R.; Manangeeswaran, M.; et al. Pseudovirus rVSVΔG-ZEBOV-GP infects neurons in retina and CNS, causing apoptosis and neurodegeneration in neonatal mice. *Cell Rep.* **2019**, *26*, 1718-1726.e4.
65. Furuyama, W.; Marzi, A.; Nanbo, A.; Haddock, E.; Maruyama, J.; Miyamoto, H.; Igarashi, M.; Yoshida, R.; Noyori, O.; Feldmann, H.; et al. Discovery of an antibody for pan-ebolavirus therapy. *Sci. Rep.* **2016**, *6*, 1–10.
66. White, K.D.; Frank, M.B.; Foundling, S.; Waxman, F.J. Effect of immunoglobulin variable region structure on C3b and C4b deposition. *Mol. Immunol.* **1996**, *33*, 759–768.
67. Fultz, P.N.; Holland, J.J. Differing responses of hamsters to infection by vesicular stomatitis virus Indiana and New Jersey serotypes. *Virus Res.* **1985**, *3*, 129–140.
68. Fultz, P.N.; Shadduck, J.A.; Kang, C.Y.; Streilein, J.W. Genetic analysis of resistance to lethal infections of vesicular stomatitis virus in Syrian hamsters. *Infect. Immun.* **1981**, *32*, 1007–1013.
69. Milligan, J.C.; Parekh, D. V.; Fuller, K.M.; Igarashi, M.; Takada, A.; Saphire, E.O. Structural characterization of pan-ebolavirus antibody 6D6 targeting the fusion peptide of the surface glycoprotein. *J. Infect. Dis.* **2019**, *219*, 415–419.
70. Fultz, P.N.; Shadduck, J.A.; Kang, C.Y.; Streilein, J.W. Mediators of protection against lethal systemic vesicular stomatitis virus infection in hamsters: Defective

interfering particles, polyinosinate-polycytidylate, and interferon. *Infect. Immun.* **1982**, *37*, 679–686.

71. Finkelshtein, D.; Werman, A.; Novick, D.; Barak, S.; Rubinstein, M. LDL receptor and its family members serve as the cellular receptors for vesicular stomatitis virus. *Proc. Natl. Acad. Sci. U. S. A.* **2013**, *110*, 7306–7311.
72. Nikolic, J.; Belot, L.; Raux, H.; Legrand, P.; Gaudin, Y.; Albertini, A.A. Structural basis for the recognition of LDL-receptor family members by VSV glycoprotein. *Nat. Commun.* **2018**, *9*, 1029.
73. Kortepeter, M.G.; Bausch, D.G.; Bray, M. Basic clinical and laboratory features of filoviral hemorrhagic fever. *J. Infect. Dis.* **2011**, *204*, S810–816.
74. Vernet, M.A.; Reynard, S.; Fizet, A.; Schaeffer, J.; Pannetier, D.; Guedj, J.; Rives, M.; Georges, N.; Garcia-Bonnet, N.; Sylla, A.I.; et al. Clinical, virological, and biological parameters associated with outcomes of Ebola virus infection in Macenta, Guinea. *JCI insight* **2017**, *2*, e88864.
75. Downs, W.G.; Anderson, C.R.; Spence, L.; Aitken, T.H.; Greenhall, A.H. Tacaribe virus, a new agent isolated from Artibeus bats and mosquitoes in Trinidad, West Indies. *Am. J. Trop. Med. Hyg.* **1963**, *12*, 640–646.
76. Simulundu, E.; Mweene, A.S.; Changula, K.; Monze, M.; Chizema, E.; Mwaba, P.; Takada, A.; Ippolito, G.; Kasolo, F.; Zumla, A.; et al. Lujo viral hemorrhagic fever: considering diagnostic capacity and preparedness in the wake of recent Ebola and Zika virus outbreaks. *Rev. Med. Virol.* **2016**, *26*, 446–454.
77. Ishii, A.; Thomas, Y.; Moonga, L.; Nakamura, I.; Ohnuma, A.; Hang'ombe, B.; Takada, A.; Mweene, A.; Sawa, H. Novel arenavirus, Zambia. *Emerg. Infect. Dis.* **2011**, *17*, 1921–1924.
78. Urata, S.; Weyer, J.; Storm, N.; Miyazaki, Y.; van Vuren, P.J.; Paweska, J.T.; Yasuda, J. Analysis of assembly and budding of Lujo virus. *J. Virol.* **2016**, *90*, 3257–3261.
79. Oppliger, J.; da Palma, J.R.; Burri, D.J.; Bergeron, E.; Khatib, A.-M.; Spiropoulou, C.F.; Pasquato, A.; Kunz, S. A Molecular sensor to characterize arenavirus envelope glycoprotein cleavage by subtilisin kexin isozyme 1/site 1 protease. *J. Virol.* **2016**, *90*, 705–714.
80. Takada, A.; Robison, C.; Goto, H.; Sanchez, A.; Murti, K.G.; Whitt, M.A.; Kawaoka, Y. A system for functional analysis of Ebola virus glycoprotein. *Proc. Natl. Acad. Sci. U. S. A.* **1997**, *94*, 14764–14769.
81. Changula, K.; Yoshida, R.; Noyori, O.; Marzi, A.; Miyamoto, H.; Ishijima, M.; Yokoyama, A.; Kajihara, M.; Feldmann, H.; Mweene, A.S.; et al. Mapping of

conserved and species-specific antibody epitopes on the Ebola virus nucleoprotein. *Virus Res.* **2013**, *176*, 83–90.

82. Maruyama, J.; Miyamoto, H.; Kajihara, M.; Ogawa, H.; Maeda, K.; Sakoda, Y.; Yoshida, R.; Takada, A. Characterization of the envelope glycoprotein of a novel filovirus, Lloviu virus. *J. Virol.* **2014**, *88*, 99–109.
83. Nakayama, E.; Tomabechi, D.; Matsuno, K.; Kishida, N.; Yoshida, R.; Feldmann, H.; Takada, A. Antibody-dependent enhancement of marburg virus infection. *J. Infect. Dis.* **2011**, *204*, S978.
84. Latysheva, N.; Muratov, G.; Rajesh, S.; Padgett, M.; Hotchin, N.A.; Overduin, M.; Berditchevski, F. Syntenin-1 is a new component of tetraspanin-enriched microdomains: mechanisms and consequences of the interaction of syntenin-1 with CD63. *Mol. Cell. Biol.* **2006**, *26*, 7707–7718.
85. Pols, M.S.; Klumperman, J. Trafficking and function of the tetraspanin CD63. *Exp. Cell Res.* **2009**, *315*, 1584–1592.
86. Sizikova, T.E.; Lebedev, V.N.; Syromyatnikova, S.I.; Borisevich, S. V. Lujo hemorrhagic fever. *Vopr. Virusol.* **2017**, *62*, 149–153.
87. Bari, R.; Guo, Q.; Xia, B.; Zhang, Y.H.; Giesert, E.E.; Levy, S.; Zheng, J.J.; Zhang, X.A. Tetraspanins regulate the protrusive activities of cell membrane. *Biochem. Biophys. Res. Commun.* **2011**, *415*, 619–626.
88. Pileri, P.; Uematsu, Y.; Campagnoli, S.; Galli, G.; Falugi, F.; Petracca, R.; Weiner, A.J.; Houghton, M.; Rosa, D.; Grandi, G.; et al. Binding of hepatitis C virus to CD81. *Science (80-.).* **1998**, *282*, 938–941.
89. Zona, L.; Tawar, R.G.; Zeisel, M.B.; Xiao, F.; Schuster, C.; Lupberger, J.; Baumert, T.F. CD81-receptor associations - Impact for hepatitis C virus entry and antiviral therapies. *Viruses* **2014**, *6*, 875–892.
90. Yang, W.; Zhang, M.; Chi, X.; Liu, X.; Qin, B.; Cui, S. An intramolecular bond at cluster of differentiation 81 ectodomain is important for hepatitis C virus entry. *FASEB J.* **2015**, *29*, 4214–4226.
91. Kinchen, V.J.; Zahid, M.N.; Flyak, A.I.; Soliman, M.G.; Learn, G.H.; Wang, S.; Davidson, E.; Doranz, B.J.; Ray, S.C.; Cox, A.L.; et al. Broadly neutralizing antibody mediated clearance of human hepatitis C virus infection. *Cell Host Microbe* **2018**, *24*, 717-730.e5.
92. VanCompernolle, S.E.; Wiznycia, A. V.; Rush, J.R.; Dhanasekaran, M.; Baures, P.W.; Todd, S.C. Small molecule inhibition of hepatitis C virus E2 binding to CD81. *Virology* **2003**, *314*, 371–380.
93. Al Olaby, R.R.; Cocquerel, L.; Zemla, A.; Saas, L.; Dubuisson, J.; Vielmetter, J.;

Marcotrigiano, J.; Khan, A.G.; Catalan, F.V.; Perryman, A.L.; et al. Identification of a novel drug lead that inhibits HCV infection and cell-to-cell transmission by targeting the HCV E2 glycoprotein. *PLoS One* **2014**, *9*, e111333.